Available online at www.sciencedirect.com
ScienceDirect
Ore Geology Reviews 30 (2007) 217–243
ORE GEOLOGY REVIEWS
www.elsevier.com/locate/oregeorev

Geology, mineralogy and stable isotope geochemistry of the Kabwe carbonate-hosted Pb–Zn deposit, Central Zambia

A.F. Kamona [a,*], G.H. Friedrich [b]

[a] *Geology Department, Science Faculty, University of Namibia, Private Bag 13301, 9000 Windhoek, Namibia*
[b] *Institut für Mineralogie und Lagerstättenlehre, RWTH Aachen, Wüllnerstrasse 2, 52062 Aachen, Germany*

Received 18 November 2004; accepted 13 February 2006
Available online 5 June 2006

Abstract

The carbonate-hosted Kabwe Pb–Zn deposit, Central Zambia, has produced at least 2.6 Mt of Zn and Pb metal as well as minor amounts of V, Cd, Ag and Cu. The deposit consists of four main epigenetic, pipe-like orebodies, structurally controlled along NE–SW faults. Sphalerite, galena, pyrite, minor chalcopyrite, and accessory Ge-sulphides of briartite and renierite constitute the primary ore mineral assemblage. Cores of massive sulphide orebodies are surrounded by oxide zones of silicate ore (willemite) and mineralized jasperoid that consists largely of quartz, willemite, cerussite, smithsonite, goethite and hematite, as well as numerous other secondary minerals, including vanadates, phosphates and carbonates of Zn, Pb, V and Cu.

Galena, sphalerite and pyrite from the Pb–Zn rich massive orebodies have homogeneous, negative sulphur isotope ratios with mean $\delta^{34}S_{CDT}$ permil (‰) values of −17.75±0.28 (1σ), −16.54±0.0.27 and −15.82±0.25, respectively. The Zn-rich and Pb-poor No. 2 orebody shows slightly heavier ratios of −11.70±0.5‰ $\delta^{34}S$ for sphalerite and of −11.91±0.71‰ $\delta^{34}S$ for pyrite. The negative sulphur isotope ratios are considered to be typical of sedimentary sulphides produced through bacterial reduction of seawater sulphate and suggest a sedimentary source for the sulphur.

Carbon and oxygen isotope ratios of the host dolomite have mean $\delta^{13}C_{PDB}$ and $\delta^{18}O_{SMOW}$ values of 2.89‰ and 27.68‰, respectively, which are typical of marine carbonates. The oxygen isotope ratios of dolomite correlate negatively to the SiO_2 content introduced during silicification of the host dolomite. The depletion in ^{18}O in dolomite indicates high temperature fluid/rock interaction, involving a silica- and ^{18}O-rich hydrothermal solution.

Two types of secondary fluid inclusions in dolomite, both of which are thought to be related to ore deposition, indicate temperatures of ore deposition in the range of 257 to 385 and 98 to 178 °C, respectively. The high temperature fluid inclusions contain liquid + vapour + solid phases and have salinities of 15 to 31 eq. wt.% NaCl, whereas the low temperature inclusions consist of liquid + vapour with a salinity of 11.5 eq. wt.% NaCl.

Fluid transport may have been caused by tectonic movements associated with the early stages of the Pan-African Lufilian orogeny, whereas ore deposition within favourable structures occurred due to changes in pressure, temperature and pH in the ore solution during metasomatic replacement of the host dolomite. The termination of the Kabwe orebodies at the Mine Club fault zone and observed deformation textures of the ore sulphides as well as analysis of joint structures in the host dolomite, indicate that ore emplacement occurred prior to the latest deformation phase of the Neoproterozoic Lufilian orogeny.

Keywords: Neoproterozoic; Carbonate-hosted; Massive orebodies; Lufilian orogeny; Base metals

* Corresponding author.
E-mail address: afkamona@unam.na (A.F. Kamona).

0169-1368/$ - see front matter © 2006 Elsevier B.V. All rights reserved.
doi:10.1016/j.oregeorev.2006.02.003

1. Introduction

The carbonate-hosted Kabwe Pb–Zn mine is located on latitude 14°27′S and longitude 28°26′E in Central Zambia, about 110 km north of Lusaka (Fig. 1). Over its lifespan of 88 years of underground mining, Kabwe mine produced 1.8 Mt of Zn and 0.8 Mt of Pb as well as minor amounts of Ag (79 t), fused V_2O_5 (7820 t), Cd (235 t) and Cu (64 t) as by-products (Kamona, 1993). Mine closure in 1994 was due to exhaustion of the Pb–Zn massive sulphide ore, but about 1.9 Mt of mainly Zn-rich silicate resources (with 13.4 wt.% Zn and 1.5 wt.% Pb) remain in situ. Renewed interest in the Kabwe deposit is due to recent advances in ore processing technologies and awareness about the economic potential of sediment-hosted deposits as sources of non-sulphide Zn (Brugger et al., 2003; Hitzman et al., 2003; Sangster, 2003) and because of the presence of relatively rare trace elements of Ge, Ga, and In, which are employed in high-technology applications (Melcher et al., 2006; Wood and Samson, 2006).

The Kabwe deposit was discovered in 1902 by T.G. Davey, who prospected the area on behalf of Northern Copper (British South Africa) Company (Spencer, 1908; Guernsey, 1953). Davey named the deposit "Rhodesia-Broken Hill" due to the resemblance of the countryside to the Broken Hill district in Australia (Bancroft, 1961; Reeve, 1963). Early publications on the geology and mineralogy of the Kabwe deposit include those of Mennell and Chubb (1907), Spencer (1908,1927), Zealley (1912), Hubbard (1913), Speak (1919), Mennell (1920a), and Pelletier (1929). Later publications reported new minerals and also included various aspects of the geochemistry of the ores and host rocks (Taylor, 1954, 1958; Coles, 1959; Dechow and Jensen, 1965; Whyte, 1966; Kortman, 1972; Notebaart and Korowski, 1980; Braithwaite, 1988). Lead isotopes of ore galena and the carbonate host rocks (Kamona et al., 1999) and preliminary results on the geology, mineralogy and geochemistry of the Kabwe deposit have been previously reported (Kamona et al., 1990; Kamona et al., 1991a,b; Kamona and Friedrich, 1994).

In this paper, additional data on the morphology of the individual orebodies and their structural setting, mineralogy, sulphur isotope geochemistry, and preliminary results of fluid inclusion studies are presented and discussed in order to provide a comprehensive overview of the Kabwe Pb–Zn deposit and its genetic characteristics. The available evidence shows that the Pb–Zn deposit may be described as an epigenetic, moderate to high temperature, carbonate-hosted type, whose origin is associated with the mobilisation of metals and fluid circulation in an intra-continental rift basin.

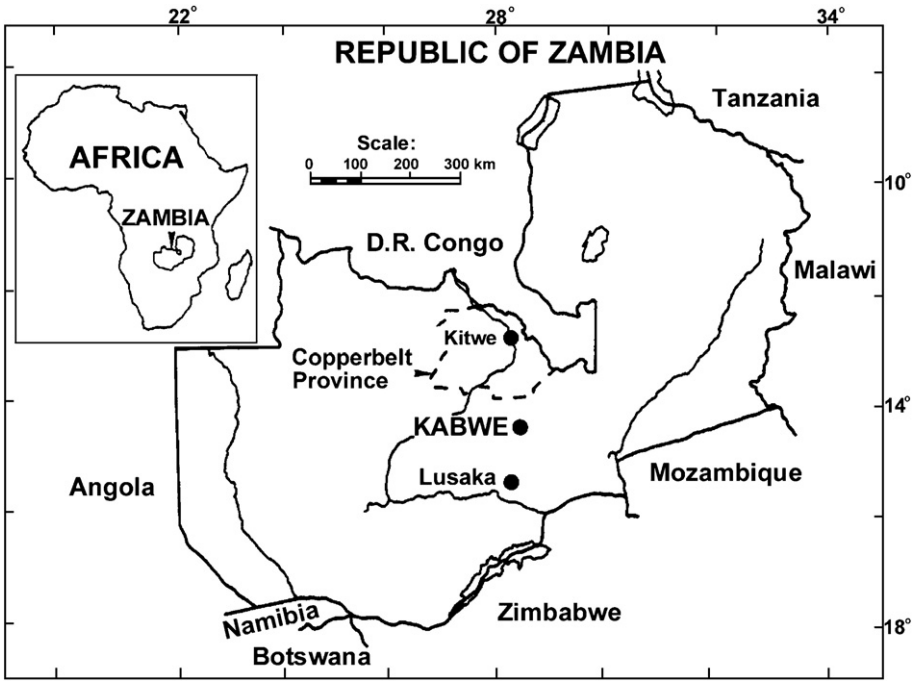

Fig. 1. Location of Kabwe in Central Zambia.

2. Regional geological setting

The Kabwe region is mostly underlain by Neoproterozoic metasedimentary cover rocks which unconformably overlie a Palaeo- to Mesoproterozoic basement of granite gneiss with minor amphibolite, schist, quartzite, pegmatite and xenolithic metasediments (Arthurs et al., 1995; Cairney and Kerr, 1998). Quartzite, schist, ironstone and banded iron formation of the Muva Supergroup flank the granite–gneiss complex. Quartz–tourmaline conglomerate and volcanic rocks of uncertain age occur within the Muva quartzite. The granite–gneiss of the Basement Complex is part of a Palaeoproterozoic magmatic arc emplaced in the range 2050 to 1865 Ma, whereas the Muva Supergroup formed between 1941 and 1355 Ma (Cahen et al., 1984; Rainaud et al., 2002a).

Metasedimentary cover rocks consist of meta-arkose, quartzite and conglomerate at the base with overlying phyllite, meta-argillite, metasiltstone, quartzite and dolomite–marble and associated tremolite schist, microdiorite, gabbro, amphibolite and epidosite (Moore, 1964; Cairney and Kerr, 1998). These rocks are generally considered to have formed within the same period as the Neoproterozoic Katangan rocks of the Copperbelt from 877 to 656 Ma (Cahen et al., 1984; Cairney and Kerr, 1998; Armstrong et al., 1999).

The cover rocks have been subdivided into the Kangomba and Nyama Formations (Table 1). The Kangomba Formation consists of an underlying quartzitic–micaceous member and an overlying, mainly dolomitic member, which corresponds to the Lower and Upper Roan Groups, respectively (Moore, 1964; Cairney and Kerr, 1998). This correlation of the Kangomba with the Roan Group suggests that deposition occurred in the period from ca. 880 to 765 Ma (Armstrong et al., 1999; Key et al., 2001). The overlying Nyama Formation, consists of dolomite– and calcite-marble and phyllite, and has been correlated to the Lower Kundelungu, but it is also possible that it is equivalent to the Upper Roan, as indicated by the structural and geochronological data of Barr et al. (1978) for the Lusaka Dolomite, which is presumably equivalent to the Nyama Formation (Moore, 1964; Cairney and Kerr, 1998).

Various lithological units of the Kangomba Formation contain base metal mineralization on a regional scale, including disseminated Cu mineralization in massive quartzite at Sebembere (Dawson, in press), and Cu–Zn mineralization in tremolite schist above footwall quartzite at Mufukushi (Cairney and Kerr, 1998). Pb–Zn mineralization of the Kabwe-type occurs in dolomite of the upper Kangomba Formation.

Table 1
Lithostratigraphic succession in the Kabwe region, after Gair (1960), Moore (1964), Arthurs et al. (1995), Cairney and Kerr (1998), and Dawson (in press)

Lithology and thickness (m)	Formation	Age
Sandstone	Upper Sandstone	Upper Triassic
Grit, sandstone, mudstone, conglomerate (2300)	Escarpment Grit	
Mudstone (900)	Madumabisa Mudstone	Upper Permian
Coal, shale, mudstone, sandstone (130)	Coal Measures	Lower Permian
Mudstone (30)	Red Mudstone	Upper Carboniferous
Conglomerate, sandstone (50)	Basal Sandstone–Conglomerate	
	Unconformity	
Andesite		Neoproterozoic
Phyllite, dolomite, marble, slate, mudstone	Nyama	
Phyllite, dolomite, slate, schist, metasiltstone, quartzite	Kangomba	
Arkose, quartzite, conglomerate, schist	*Unconformity*	
Schist, ironstone, quartzite	Chisamba	Palaeo- to Mesoproterozoic
Quartzite, schist, banded iron formation, conglomerate	Chikonkomene	
	Unconformity	
Granitic-gneiss, schist, amphibolite	Mwomboshi Gneiss	Palaeoproterozoic

Three successive deformation phases resulting from the Lufilian orogeny have been recognised within the metasedimentary cover rocks (Moore, 1964; Cairney and Kerr, 1998). The earliest fold phase is characterised by N–S trending isoclinal folds with a shallow to moderate southerly plunge, whereas a later phase is defined by minor open folds with NNW–SSE axes. The latest deformation phase resulted in E–W to NE–SW trending regional anticlinal and synclinal structures within both the basement and cover rocks. This final phase generally resulted in refolding and refoliation of older structures.

Porada and Berhorst (2000) have pointed out that there is inadequate age data in the Lufilian Belt to support the occurrence of three deformation phases. In their tectogenetic model for the Lufilian and Zambezi belts, only one major collisional event, the Katanga Orogeny, occurred at ca. 550 Ma (Porada and Berhorst, 2000). However, geological mapping in the Lufilian Arc, including the work of Cosi et al. (1992) and Key et al. (2001) in northwest Zambia, has consistently shown evidence of three deformation phases. The oldest metamorphic event is recorded by biotite K–Ar ages in the range 708±7 to 628±7 Ma in the Domes area (Cosi et al., 1992). More recent SHRIMP U–Pb age data

on monazite from the Chambishi basin indicate three metamorphic events with ages of 592 ± 22, 531 ± 12, and 512 ± 17 Ma, respectively (Rainaud et al., 2002b).

According to De Swardt et al. (1965), regional shear zones developed at the end of the Lufilian Orogeny when compressive stresses ruptured the basement along ENE trends determined by the Irumide orogeny. The Muva Supergroup quartzite–schist–metavolcanic sequences are bounded by faults, including E–W trending thrust faults sub-parallel to the Mwembeshi shear zone (MSZ) (Moore, 1964). Normal NW–SE trending faults occur northwest of Kabwe (Cairney and Kerr, 1998). The precise age of the faulting is uncertain, but it is considered to post-date the final Lufilian fold phase.

Effects of both amphibolite and greenschist facies regional metamorphism have been recognised in the area (Moore, 1964; Ramsay and Ridgway, 1977; Arthurs et al., 1995; Cairney and Kerr, 1998). The presence of kyanite in quartz–kyanite and quartz–kyanite–garnet schist intercalated with the granitic gneiss of the basement indicates medium-pressure type of regional amphibolite facies metamorphism. Greenschist facies metamorphism occurs in both the metasedimentary and basement rocks, but it is more characteristic of the former. The mineral assemblages in the gneisses indicate retrograde metamorphism from upper amphibolite (muscovite and epidote absent) to epidote–amphibolite facies as shown by the replacement of hornblende by epidote, whereas the metavolcanic rocks intercalated with basement quartzite show a typical greenschist facies mineral assemblage of chlorite, epidote, actinolite and quartz (Arthurs et al., 1995).

The regional greenschist facies of the cover rocks is characterised by the chlorite–muscovite–biotite–quartz mineral paragenesis in phyllite and tremolite–phlogopite–dolomite schist in which poikiloblastic tremolite replaces dolomite (Cairney and Kerr, 1998). Carbonate rocks generally exhibit a low metamorphic state as indicated by the presence of talc in fine-grained recrystallized calcite-dolomite mosaics, whereas quartzite is generally sericitic and contains elongated quartz grains as well as fine-grained sutured quartz mosaics with coarser grained, strained quartz (Moore, 1964; Cairney and Kerr, 1998). More intensely deformed and recrystallized quartzite, conglomerate and quartz–muscovite schist occur along the shear zones.

3. Methodology

Geological and structural data presented in this paper is based on underground geological mapping, and core and chip sampling carried out in Kabwe prior to its closure in 1994. A total of 424 samples, including hand specimens and chip samples, was collected, mainly in and around the No. 1, No. 2, No. 3/4, No. 5/6 and No. 8 orebodies. Sample materials from other deposits and mineral occurrences near Kabwe were also collected for comparative study. This includes material from Airfield, Foundry and core samples from Sebembere (Kabwe West).

Ore and petrographic microscopes for reflected and transmitted light were used for the identification and determination of mineralogical phases and textures of the opaque and transparent phases, respectively. Doubly polished slices (100 μm thick) were used for fluid inclusion investigations in sphalerite, quartz and dolomite. The microthermometric data was determined on a heating/cooling stage from FLUID INC. (Denver, Colorado) with a measuring range from −196 to 600 °C in combination with a Zeiss microscope and a Leitz L50 objective. The error associated with the measurements was ±3 °C for homogenisation temperatures and ±0.3 °C for melting temperatures.

Ground powdered samples of rocks and minerals were prepared for X-ray diffraction (XRD) analyses to identify the mineral phases and check the purity of mineral separates used in mass spectrometry determinations. The XRD analyses were carried out with a Siemens D 500 instrument using Cu K-alpha X-rays with a wavelength of 1.5405 Å. The analyses were made between 2θ angles of 2 and 72 with voltage and current settings of 40 kV and 30 mA, respectively.

Mineral compositions of the primary sulphide phases and of dolomite were determined by means of an ARL-SEMQ electron microprobe with a modified MAGIC IV correction programme (Colby, 1968). Counting times during analysis for the concentration of elements varied from 10 to 60 s using voltages of 20 to 25 kV and a current of 15 to 20 nA.

Mineral fractions of sphalerite, galena, pyrite and dolomite for mass spectrometry analyses were separated by hand picking from sieved fractions in the size ranges 0.63 to 0.355 and 0.355 to 0.20 mm by means of a high magnification binocular microscope. The stable isotope analyses were carried out at the Scottish Universities Research and Reactor Centre in Glasgow. The sulphur isotopes of galena, sphalerite and pyrite were determined following the method of Robinson and Kusakabe (1975), and measurements of the isotope ratios were made relative to the Canyon Diablo troilite (CDT) standard with a typical laboratory precision of ±0.25‰ (1σ).

The isotopes of carbon and oxygen in mineral separates of dolomite were determined following the acid decomposition method of McCrea (1950). The results are reported as

$\delta^{13}C_{PDB}$ and $\delta^{18}O_{SMOW}$ ratios with respect to the standards Peedee belemnite (PDB) and Standard Mean Ocean Water (SMOW), respectively. The typical laboratory precision is better than ±0.1‰ (1σ) for both $\delta^{13}C$ and $\delta^{18}O$.

4. Mine geology

In the immediate Kabwe–Sebembere area (Fig. 2), granitic gneiss of the basement is composed of orthoclase, plagioclase, microcline, quartz, minor biotite and muscovite, and accessory zircon. The gneiss is unconformably overlain by arkose and quartzite of the basal Arkose–Quartzite Formation with intercalated conglomerate and schist. The Arkose–Quartzite Formation is up to 700 m thick and hosts disseminated stratiform Cu mineralization at Sebembere (Dawson, in press). It is succeeded by phyllite with minor metasiltstone, quartzite and intrusive epidosite.

The NW–SE trending band of the Kabwe Dolomite Formation (Fig. 2) consists of a massive, light grey dolomitic marble that forms the core of the Kabwe syncline with an estimated thickness of 870 m. Five members make up the formation (Kortman, 1972): (1) arenaceous dolomite, (2) micaceous dolomite, (3) schistose dolomite, (4) carbonaceous dolomite, and (5) massive dolomite. With the exception of the arenaceous dolomite, all dolomite types are exposed in the underground workings, but due to their transitional nature and the absence of definite lithological boundaries, only the schistose dolomite is delineated from the massive dolomite in mine plans and sections.

The main ore-bearing lithology is the massive dolomite member, but disseminated Pb–Zn mineralization also occurs, in places, in the carbonaceous dolomite member, such as at the Airfield deposit. The massive dolomite forming the central part of the Kabwe syncline is typically light grey and fine-grained with a blocky structure due to jointing. It is at least 215 m thick and is normally homogeneous, but may be locally banded such as on the 1250 ft level of the No. 2 orebody. At the orebody contacts the dolomite is commonly silicified and, in places, it is completely transformed to jasperoid.

The schistose dolomite is well exposed in the underground workings and is characterised by intercalations of talc-, chlorite- and phlogopite-rich domains within dolomite. It is typically white to light green and occurs in faulted contact with the massive dolomite along the Mine Club fault zone where it dips at about 55°W. Well developed cubic crystals of pyrite are common within the schistose dolomite, but apart from minor secondary oxide ore at the contact with Pb–Zn mineralization in massive dolomite, the schistose dolomite is barren. The restricted occurrence of the schistose dolomite along the Mine Club fault zone and the presence of talc suggest that it is probably a product of metasomatic alteration of an impure dolomite during faulting.

4.1. Tectonic structures

The Kabwe Dolomite Formation forms an overturned 2 km wide, 16 km long band of dolomites with a regional dip of 70°NE in a NW-plunging isoclinal

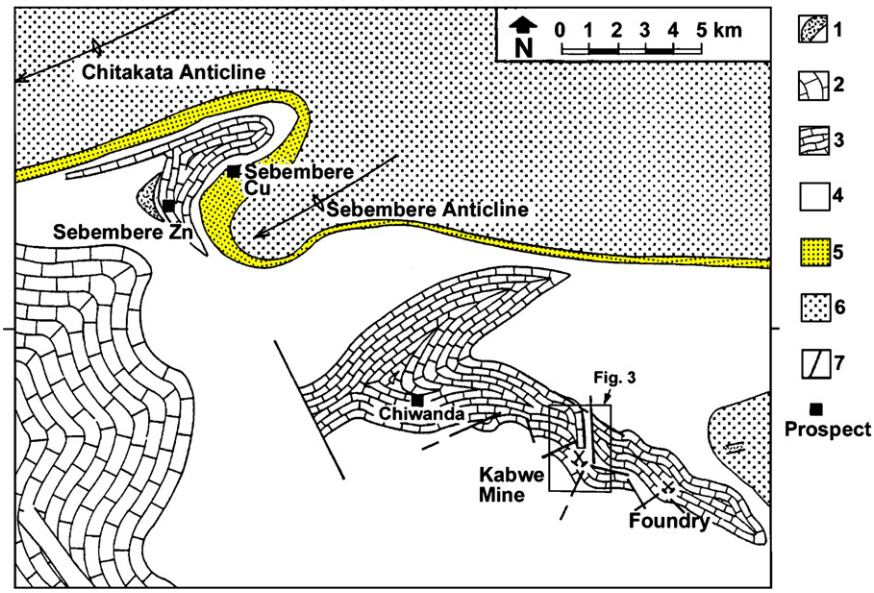

Fig. 2. Geological map of the Kabwe–Sebembere area (modified from Cairney and Kerr (1998)).

syncline (Cairney and Kerr, 1998; Tuke, in press). The surrounding phyllites typically strike E–W or NW–SE with dips of 35° to 70°N or NE. The NW–SE trend of the dolomite band changes to NE–SW near Chiwanda (Fig. 2), probably as a result of faulting associated with the Nyama dislocation shear zone of De Swardt et al. (1965).

Minor cross folds with axes that generally trend E–SW to ENE–WSW and plunges of 0° to 20°SW or NE are common (Taylor, 1954; Tuke, in press), particularly in the schistose dolomite on the southern margin of the dolomite band. More steeply dipping folds and drag-folds are sub-parallel to the Kabwe syncline and trend NW–SE or NNW–SSE with plunges of up to 60°. These folds correspond to the two periods of folding recognised by Whyte (1966), which in turn correlate to the regional F2 and F3 Lufilian fold phases of Cairney and Kerr (1998). During the F2 phase the rocks were isoclinally folded on a gently plunging NW axis represented by the NW-trending Kabwe syncline. The later F3 phase produced folds with ENE-plunging axes.

4.2. Morphology and structure of the Kabwe orebodies

Mineralization at Kabwe consists of three main massive sulphide orebodies termed the No. 1, No. 3/4, and No. 5/6, which all occur within the highly faulted part of the massive dolomite near the Mine Club fault zone (Fig. 3). The No. 2 is also a massive orebody, but it is silicate-rich and Pb-poor with willemite as the predominant ore mineral. Minor orebodies ('X', 'E', South Orebody, No. 2 Hangingwall, No. 8) are found in close proximity to the main massive sulphide orebodies, to which they may be connected. Other ore occurrences include the small, willemite-rich Foundry orebody about 3.5 km south-east of Kabwe mine (Fig. 2), and the Airfield orebody (Fig. 3), which is the only disseminated ore type in the area.

The main massive orebodies (Fig. 4) all have a pipe- to vein-like morphology with average orebody thicknesses and strike lengths ranging from 10 to 30 m and from 79 to 163 m, respectively. The orebodies generally strike north-east with subvertical dips and have a general north-east trend with plunges between 28° and 60°. The pipe-like orebodies generally consist of a sulphide core of primary sphalerite, galena and pyrite surrounded by silicate ore, predominantly willemite, and an outermost zone of jasperoid, locally termed "brown lithified mud". The ratio of sulphide to silicate ore is generally about 1:1 (Whyte, 1966), except in the No. 2 and No. 8 orebodies, which consist mainly of willemite and massive sphalerite ore, respectively.

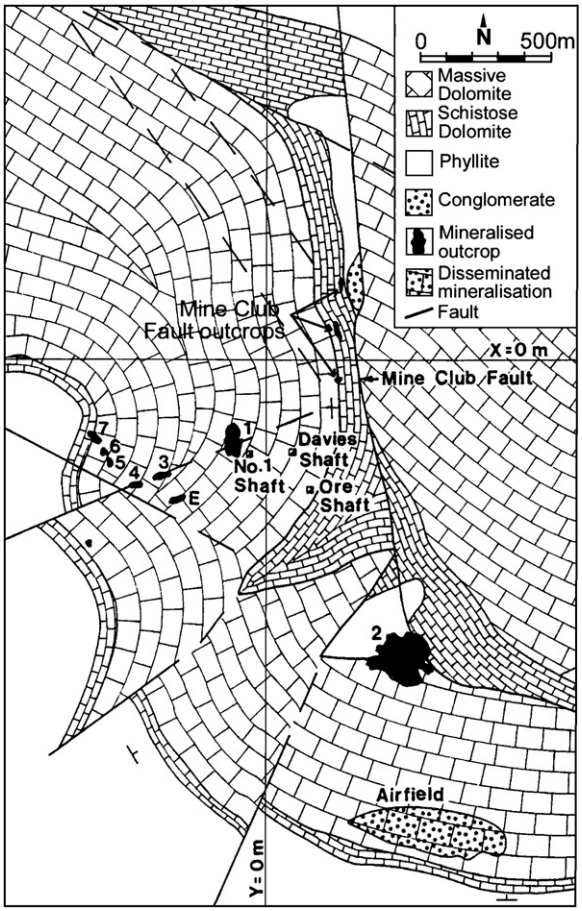

Fig. 3. Outcrop pattern of orebodies in the Kabwe mine area, based on data from Taylor (1954), Whyte (1966), Tuke (in press) and Kabwe mine.

4.2.1. The No. 1 orebody

The No. 1 orebody originally cropped out on surface as a 15 m high gossan of ferruginous, silicified dolomite with impregnations of cerussite, hemimorphite and goethite with minor smithsonite (Zealley, 1912). Crystal-lined caverns in the lower part of the gossan contained mammalian bone deposits and associated phosphates (pyromorphite, hopeite, parahopeite and tarbuttite) and vanadates (descloizite and vanadinite) (Mennell and Chubb, 1907; Spencer, 1908; Zealley, 1912; Pelletier, 1929). The dolomite underlying the gossan contained disseminations, patches and veinlets of sphalerite, galena, pyrite and chalcopyrite (Zealley, 1912), attesting to the existence of primary sulphide mineralization at depth.

Opencast mining of the mainly cerussite–hemimorphite ore from the No. 1 Kopje (Spencer, 1908) revealed that the Kopje branched into two orebodies on the 180 ft

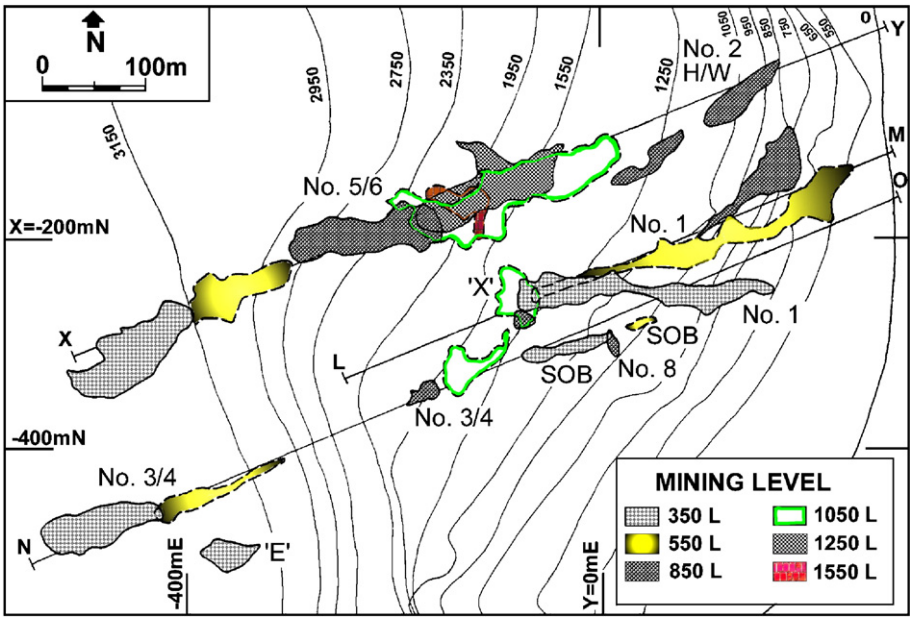

Fig. 4. Composite contour plan of the No. 1, No. 3/4, No. 5/6 and associated minor orebodies (No. 8, SOB, "E", "X" and No. 2 H/W) on various mining levels in relation to the massive dolomite/schistose dolomite contact between 0 and 3150 feet below surface. The locations of section lines X–Y, L–M and N–O (Fig. 5) are indicated.

level (the No. 1 and South Orebody; Fig. 5). The No. 1 orebody has a well developed vein form whose strike varies with depth from E–W to NE–SW with depth (Fig. 4). At its western end, the dip of the orebody is subvertical and sub-parallel to that of the host dolomite, but the dip gradually changes from 88° to 42°NW at the eastern end, where the orebody is discordant to the host dolomite. The size of the orebody generally increases with depth down to the 550 ft level, below which it decreases and eventually terminates at the contact with the schistose dolomite.

4.2.2. The No. 3/4 orebody

The No. 3/4 orebody originally cropped out as two separate orebodies, the No. 3 and No. 4 (Fig. 3), which combined at a shallow depth to form a single orebody (Whyte, 1966). The tabular orebody is discordant to the host dolomite, which dips 60° to 70°NW. The orebody varies from pipe- to vein-like with a consistent strike of 067° and sub-vertical dips between the 250 and 1050 ft levels (Figs. 4 and 5). On the 1090 ft level the strike changes to 035° and the orebody plunges southeast at 06°. Below the 750 ft level the orebody increases in size down to the 1090 ft level where its eastern extension joins the "X" orebody. It pinches out below the 1120 ft level where it terminates about 40 m above the massive dolomite/schistose dolomite contact (Fig. 5b).

4.2.3. The No. 5/6 orebody

The No. 5/6 orebody originally cropped out as two low hills (Fig. 3), less than 3 m high, which were termed the No. 5 and No. 6, respectively (Whyte, 1966; Mennell, in press). The two hills turned out to be the limbs of the largest single orebody at Kabwe with a total tonnage of 6.1 million tonnes (Mt) with average grades of 28.8 wt.% Zn and 16.1 wt.% Pb (Table 2). The strike of the No. 5/6 orebody (067°) is parallel to that of the No. 3/4 (Fig. 4) and the orebody is clearly discordant to the host dolomite, which has a local strike and dip of 290/65°NE. The pipe-like orebody is chimney-like (subvertical) below the 1050 ft level (Fig. 5c). It attains its maximum size on the 1050 ft level where it occupies an area of about 8000 m^2. Below this level the orebody decreases in size until it pinches out below the 1550 ft level, close to the schistose dolomite/massive dolomite contact. An eastern extension of the orebody on the 850 ft level (Fig. 4) is connected to the No. 2 H/W orebody above the 850 ft level.

4.2.4. The No. 2 orebody

The No. 2 orebody is located 1 km SE of the main group of massive sulphide orebodies (Fig. 3). It originally formed the largest hill-outcrop, rising 30 m above the ground surface (Pelletier, 1929). After partial mining to the 400 ft level (Taylor, 1954), further mining was abandoned in preference to orebodies with higher

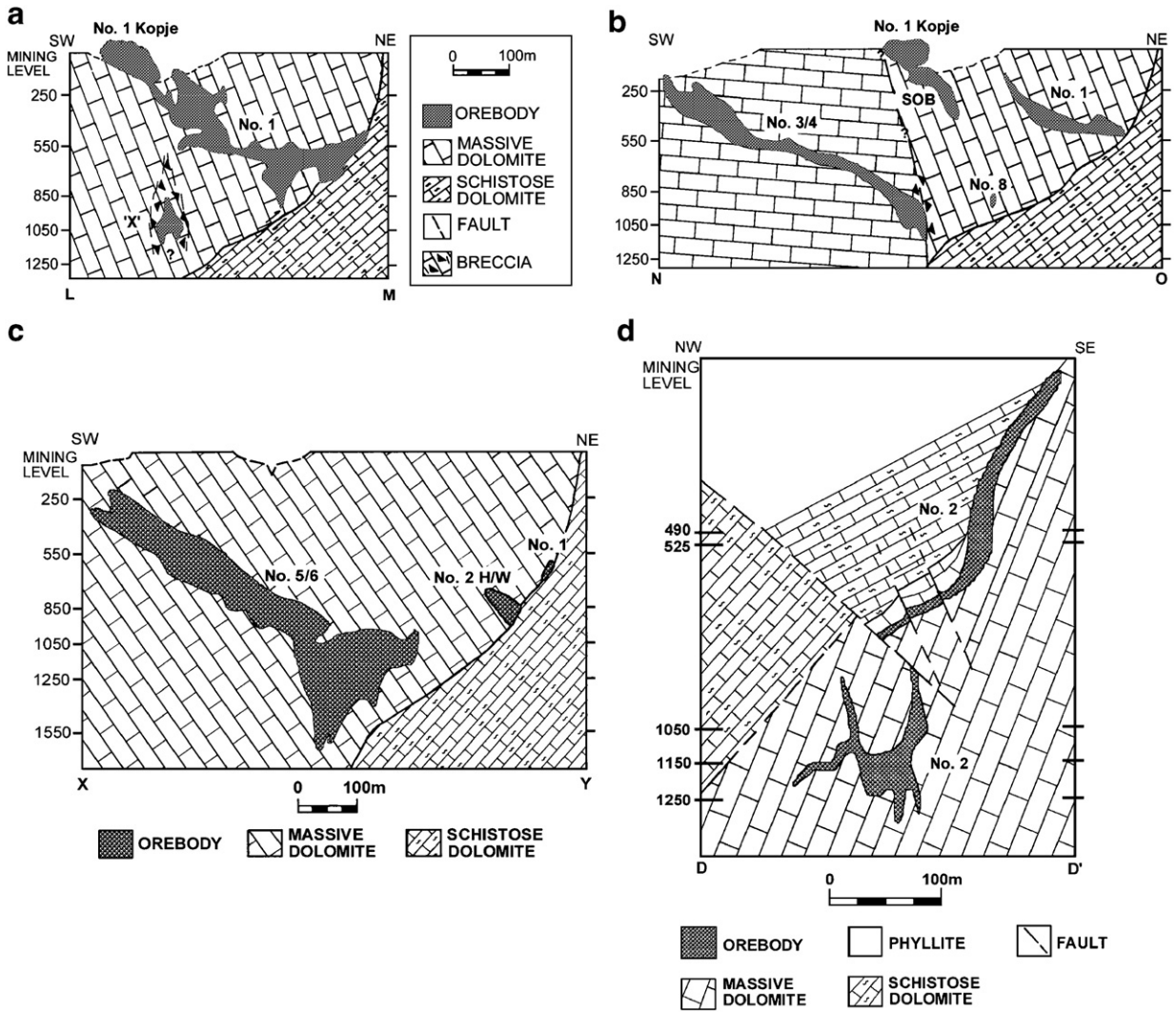

Fig. 5. Sections through the Kabwe orebodies. (a) Section L–M of the No. 1 Kopje, No. 1 and "X"; (b) Section N–O of the No. 1 Kopje, SOB, No. 1 and No. 3/4 with the projected position of the No. 8; (c) Section X–Y of the No. 5/6 and No. 2 H/W; (d) NW–SE cross-section of the No. 2 orebody.

grades of Pb. From surface down to the 550 ft level the orebody is pipe-like, but it has a more complicated structure with variable strike and dip below the 550 ft level (Fig. 5d). On the 1050 ft level it forms two separate bodies that join at depth to form a single orebody on the 1250 ft level. The structure of the No. 2 on the 1050 and 1250 ft levels appears to have been partly controlled by the host dolomite, which strikes E–W and dips at 80°N, and partly by joint sets trending NE–SW and NW–SE. The hanging wall of the eastern end of the orebody down to the 525 ft level occurs along an E–W trending shale/dolomite contact, but the rest of the orebody is entirely in massive dolomite. The lower limit of the orebody has not been exposed, but it extends down to below the 1650 ft level and thus represents the deepest occurrence of ore at Kabwe. 1.9 Mt of the No. 2 orebody grading 13.4 wt.% Zn and 1.5 wt.% Pb still remain in situ.

4.2.5. The Airfield orebody

The Airfield orebody (Fig. 3) is different from all other orebodies at Kabwe in that it contains disseminated sulphides and a lateritic blanket of silicate ore rather than massive sulphide or silicate mineralization. The disseminated sulphides occur in micaceous bedrock dolomite close to surface and include narrow zones (1 to 3 m wide) of high grade ore with up to 12 wt.% Zn + Pb (Haldane, in press-a). The silicate blanket ore occurs as thin (1.3 m) horizontal bodies that form the basal part of a lateritic "B" soil horizon and are composed of

Table 2
Estimated pre-production tonnages and grades of orebodies at Kabwe (based on mine data)

Orebody	Tonnes ($\times 10^3$)	Zn (wt.%)	Pb (wt.%)	Zn/(Zn + Pb)
No. 1	2352	26.6	18.0	0.60
No. 2	2079	14.2	1.5	0.90
No. 3/4	1112	28.7	18.4	0.61
No. 5/6	6105	28.8	16.1	0.64
"X"	205	27.7	18.8	0.60
SOB	112	34.7	9.5	0.79
"E"	70	22.0	5.0	0.81
No. 2 H/W	54	19.3	6.4	0.75
No. 8	27	62.7	0.9	0.99
Airfield	4565	2.5	1.4	0.64

hemimorphite, cerussite, descloizite, pyromorphite, smithsonite and Pb–Zn bearing Fe–Al- and Mn-oxides (Haldane, in press-a). Massive pods of coarse-grained galena encrusted with quartz are commonly associated with the mineralization. The pods of galena have apparently formed in the cementation zone.

4.2.6. The "X" orebody

The "X" orebody (Fig. 5a) was intersected underground between the 850 and 1180 ft levels. It consists of several pipe-like lenses in contact with each other (Kortman, 1972) and both the orebody and the surrounding dolomite are brecciated (Whyte, 1966). The breccia consists of angular fragments of dolomite set in a chert-like matrix (Coles, 1959). The orebody lenses out in a series of "tooth-like" bodies (Whyte, 1966) below the 1050 ft level. During this study it was observed that the "X" orebody is connected to the 3/4 orebody on the 1090 ft level and it is therefore not a blind orebody as such.

4.2.7. The South Orebody

The South Orebody (SOB) is a minor pipe-like body situated 50 m south of the No. 1 orebody (Fig. 4). It was originally connected to the No. 1 Kopje above the 180 ft level (Coles, 1959; Fig. 5b). It has a vertical dip and a strike of 074° with a trend and plunge of 074/37° between the 250 and 550 ft levels. The orebody decreases in size below the 350 ft level down to the 650 ft level where it was thought to pinch out, but its continuation was later intersected by diamond drilling below the 750 ft level.

4.2.8. The "E" orebody

The "E" orebody occurs 60 m south of the No. 3/4 (Fig. 4). Its morphology varies from pipe-like to vein-like with depth and it apparently joined the No. 3/4 on the 450 ft level (Coles, 1959). The orebody strikes NE–SW and dips 50° NW, towards the No. 3/4 and its northwest plunge at 43° is different from the common NE-trend of most orebodies. It has an average thickness of 14 m and diminishes in size with depth until it pinches out below the 400 ft level.

4.2.9. The No. 2 H/W orebody

The No. 2 H/W orebody (Fig. 4) occurs just below the 750 ft level and pinches out on the 910 ft level. It is connected to the eastern extension of the No. 5/6 orebody above the 850 ft level and is thus a continuation of the latter. The orebody has an average thickness of 17 m with a maximum strike length of 95 m and it terminates at the schistose dolomite contact (Fig. 5c).

4.2.10. The No. 8 orebody

The No. 8 orebody is known between the 760 and 910 ft levels where it has a strike and dip of 343/90°. It plunges north at 60° (Kortman, 1972) and has an average thickness of 7 m and a strike length of 21 m on the 850 ft level (Fig. 4). The orebody is unusual in that it is the only one consisting of massive sphalerite without a surrounding oxide zone. Instead, it is enclosed within a white to pink, coarse-grained variety of massive dolomite.

4.3. Other ore occurrences

Other minor occurrences of ore include the Foundry orebody (Fig. 2) and the Mine Club outcrops (Fig. 3). The small Foundry orebody consists of six pipe- to vein-like, irregularly shaped, discrete outcrops associated with faults (Tuke, in press; Haldane, in press-b). It occurs in the lower part of the dolomite near the contact with underlying phyllite and consists mainly of willemite with irregular patches of sphalerite and galena. The host dolomite forms a NW-plunging syncline flanked by NW–SE-striking phyllite that dips 50°NE. The Foundry outcrops strike E–W with sub-vertical dips and shallow eastward plunges. The outcrops have not been explored in detail and it is not known whether they are a capping to major pipe-like bodies at depth or represent discrete pods (Haldane, in press-b).

The Mine Club outcrops occur along the Mine Club fault on the schistose dolomite/massive dolomite contact (Fig. 3). They have not been developed and consist mostly of silicate ore similar to the No. 2 orebody.

4.4. Tonnage and grade

The estimated pre-production tonnage and grade data of the major and minor orebodies at Kabwe are

summarised in Table 2. The tonnage of the massive sulphide orebodies ranges from 27,000 t (No. 8) to 6.1 Mt (No. 5/6), whereas the silicate-rich orebodies range from 5000 t (Foundry) to 2.1 Mt (No. 2). The variable size of the orebodies makes it particularly difficult to locate small orebodies during exploration drilling.

The ore grades vary from Zn-rich, with metal ratio Zn/(Zn + Pb) > 0.7, to Pb–Zn dominant with metal ratios around 0.6. Apart from the No. 8 orebody, which consists of sphalerite mineralization, the Zn-rich ore is predominantly composed of willemite, the so-called "silicate ore", and has an average metal ratio of 0.85, whereas the Pb–Zn ore is more sulphide rich and contains significant Pb in the form of galena. About 65,000 t of the Airfield deposit consist of lateritic blanket ore with grades of 16.0 wt.% Zn and 5.0 wt.% Pb (Haldane, in press-a). The Zn/(Zn + Pb) metal ratio of the lateritic blanket ore (0.76) is similar to that of the silicate-rich ore, whereas the metal ratio of the disseminated sulphide ore (0.64) is more comparable to that of the massive sulphide ores.

The similarity in metal ratios of the disseminated sulphide mineralization of the Airfield deposit and the massive sulphide orebodies ("X", No. 3/4, No. 1, and No. 5/6), indicates a broadly similar mineralizing solution for these two types of mineralization. In contrast, the metal ratio of the lateritic blanket ore, which is similar to that of the silicate-rich ores, indicates that subsurface oxidation of the primary ore led to Zn enrichment relative to Pb in these ores.

5. Ore mineralogy and geochemistry

The main massive sulphide orebodies consist principally of sphalerite, galena, and pyrite with minor to trace amounts of chalcopyrite, rare briartite [$Cu_2(Fe,Zn)GeS_4$], and renierite [$(Cu_{3-x})Ge_xFeS_4$]. The sulphide ore forms the cores of the massive orebodies which are commonly enclosed in zones of oxide ore that extend up to the wallrock contacts. Remnants of massive sulphide bodies have been observed in marginal zones of some oxidised orebodies such as the No. 5/6 and No. 2. Jasperoid bodies occur in the marginal zones of some orebodies and occasionally within them as in the No 5/6 and No. 3/4. Blocks of massive dolomite that have apparently escaped replacement, are also found within the orebodies.

5.1. Sphalerite

Sphalerite (ZnS) is an ubiquitous sulphide in all the orebodies at Kabwe and it is the most abundant ore mineral on a deposit scale. It forms massive orebodies along with galena and pyrite, and also occurs as monominerallic pods up to 0.5 m across within the major orebodies. One minor orebody (No. 8) is composed entirely of coarse-grained sphalerite. Sphalerite is also disseminated in the host-rock massive dolomite and in the carbonaceous dolomite. Mineral banding caused by millimetre-wide interbands of galena and sphalerite (No. 5/6, 3/4, and No. 1 orebodies) or of sphalerite and pyrite (No. 2 orebody) occurs locally on a macroscopic scale.

Sphalerite is typically honey-yellow, anhedral to subhedral, medium-grained (< 1–2 mm), and occurs as massive aggregates in sphalerite-rich ore (Fig. 6a) or as disseminated grains with a granoblastic-polygonal texture (Fig. 6b). Fine-grained sphalerite (≤ 0.5 mm) is frequently enclosed in pyrite and, in places sphalerite also encloses grains of pyrite, briartite and renierite. In the partially oxidised ore and cementation zones, sphalerite is replaced along grain boundaries, fractures, and crystallographic planes by galena, smithsonite, and willemite (Fig. 6a, c, d). Deformation of sphalerite is indicated by grain fracturing and lamellar twinning.

Minor to trace amounts of Fe, Cd, and Mn substitute for Zn in the sphalerite lattice. The mean Fe content in 182 sphalerite analyses was found to be 1.06 wt.% with a narrow range from 0.29 to 1.89 wt.% Fe. The mean Fe content corresponds to 1.85 mol% FeS with a range from 0.51 to 3.27 mol% FeS. The mean Cd value in sphalerite is 0.16 wt.% with minimum and maximum contents of 0.08 and 0.41 wt.% Cd, respectively. The Mn content is negligible (0.01 to 0.11 wt.%) with a mean value of only 0.05 wt.% Mn.

5.2. Galena

Galena (PbS) is a major ore sulphide in the Pb-rich orebodies (No. 5/6, No. 3/4 and No. 1), but it is a minor to accessory phase in the No. 2 orebody, which consists largely of oxidised ore. Galena is interstitial to sphalerite in the sphalerite-rich ore (Fig. 6a) and is generally homogeneous and free of other mineral inclusions, but it may fill pores in pyrite. It appears to have formed late in the paragenetic sequence as it commonly forms a matrix to the other sulphides (Fig. 6b) and replaces chalcopyrite and renierite (Fig. 7c). Deformation of galena is indicated by bent cleavage planes and by grain fracturing.

A second generation of galena (galena 2) commonly forms rim overgrowths around sphalerite and replaces it along fractures and crystallographic planes (Fig. 6c). This secondary galena is abundant in the cementation zone where it is intergrown with covellite and chalcocite. Galena is itself replaced by cerussite, which is characterised by relict inclusions of galena (Fig. 6c).

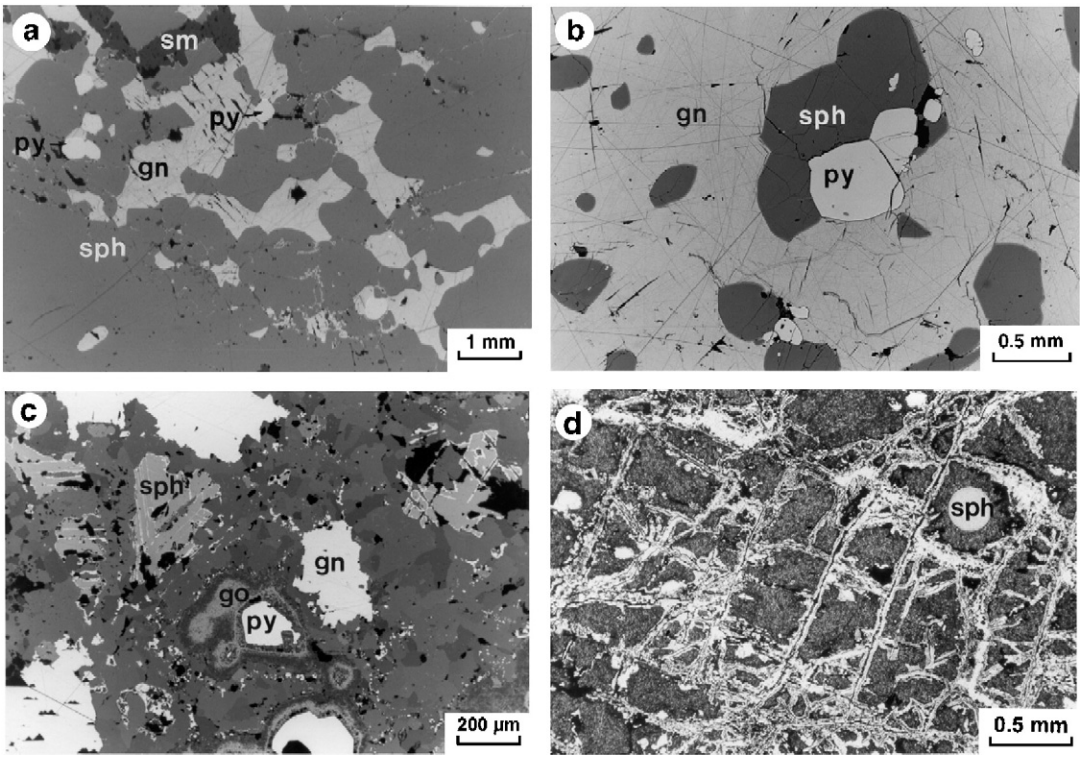

Fig. 6. Photomicrographs of massive ore textures. (a) Sphalerite (sph) with interstitial galena (gn) and disseminated pyrite (py). Smithsonite (sm) partly replaces sphalerite; No. 1 orebody, 910 ft level. (b) White galena with disseminated grains of grey anhedral sphalerite and pyrite; No. 3/4 orebody, 1090 ft level. (c) Replacement texture of anhedral relics of galena, sphalerite and pyrite in a dark grey matrix of cerussite and smithsonite. Galena and goethite (go) also replace sphalerite and pyrite, respectively; No. 3/4 orebody, 1106 ft level. (d) Cellular boxwork replacement of sphalerite by willemite and minor intergrown smithsonite (both white/grey) with goethite (dark grey) in central zones. Galena (black) rims some sphalerite grains; No. 3/4 orebody, 1118 ft level.

Galena has a uniform composition and no significant differences were observed in galena from the different mineral parageneses. Apart from Bi and Ag, the concentrations of other trace elements (Sb, Cu, As, Zn, Se) in galena are negligible with maximum values below their respective detection limits. Bi and Ag occur in low amounts, averaging only 0.06 and 0.03 wt.%, respectively in the 90 analyses made.

5.3. Pyrite

Pyrite is subordinate to sphalerite and galena in the massive sulphide ores, where it is disseminated as subhedral grains (≤1 mm) (Fig. 6a, b). However, it forms massive monomineralic zones in the No. 5/6 orebody (880 and 910 ft levels) and in the No. 2 orebody on the 525 ft level. A banded texture of pyrite and sphalerite was observed in the No. 2 orebody (1250 ft level). Deformed pyrite shows a cataclastic texture in fractured zones, 2 to 4 mm in width, in the massive pyrite bodies.

Apart from rare, fine-grained sphalerite inclusions (<0.01 to 0.02 mm), massive pyrite is typically inclusion free, whereas disseminated pyrite in the sphalerite–galena ores encloses fine-grained galena, sphalerite, and more rarely, briartite and renierite. Pyrite is partially to completely replaced by goethite and hematite, which typically form colloform aggregates, boxwork structures and cubic pseudomorphs after pyrite (Fig. 6c). Quartz may fill vugs in partly oxidised zones of massive pyrite mineralization. Where oxidation is complete, pyrite has been replaced by massive goethite and hematite, forming a dark reddish brown to grey rock locally termed “ironstone”.

Most of the trace elements analysed for in pyrite (As, Co, Ni, V, Au, Ag, Sb) occur in concentrations generally below their respective detection limits, except for Co and Ni. The Co content varies from 0.04 to 0.11 wt.% with an average of 0.07 wt.%. The Co concentration is consistently greater than that of Ni, which is more constant with an average of 0.02 wt.% Ni. The Co/Ni ratio

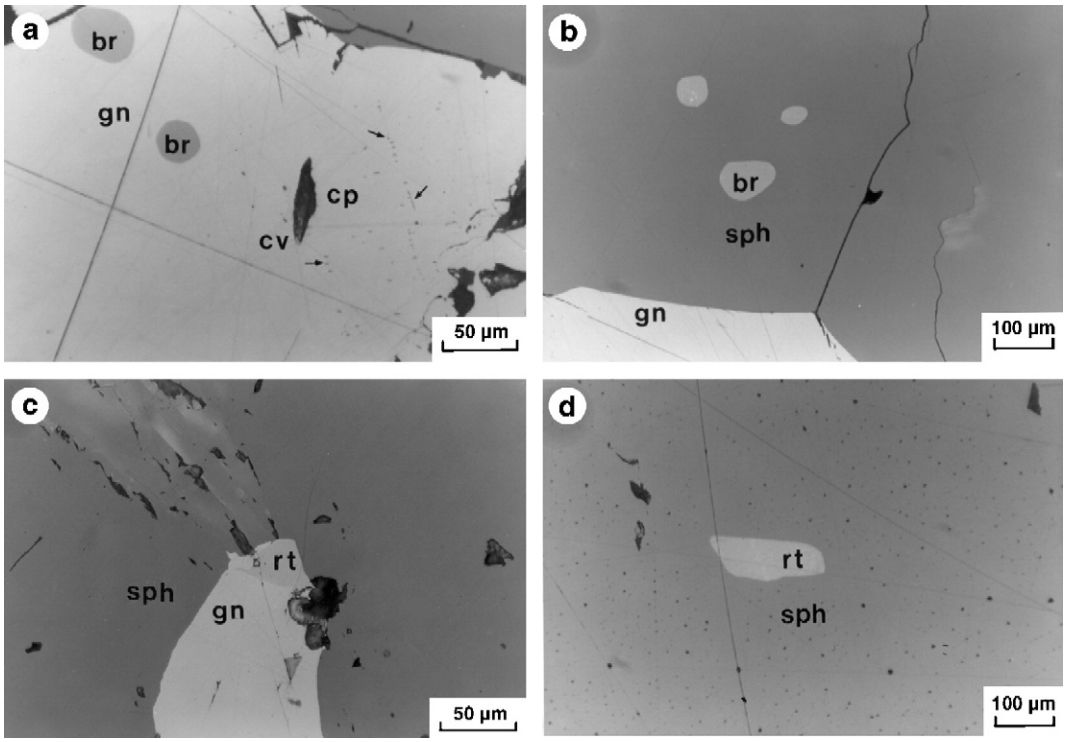

Fig. 7. Photomicrographs of germanium sulphides. (a) Light grey rounded briartite grains (br) in a galena matrix and as oriented blebs (arrows) in chalcopyrite (cp). Fractured grey sphalerite (sph) is in contact with galena and dark grey covellite (cv) replaces chalcopyrite, No. 3/4 orebody, 1106 ft level. (b) Rounded briartite grains in sphalerite; the top left briartite grain contains inclusions of chalcopyrite (white) and white galena forms a straight to curved boundary with sphalerite, No. 3/4 orebody, 1106 ft level; (c) Renierite (rt) intergrown with and partly replaced by galena. Both minerals are enclosed in sphalerite; No. 1 orebody, 910 ft level. (d) Renierite in a grey sphalerite matrix; No. 1 orebody, ft level.

averages 3.96 with a range from 1.61 to 9.42. The range in the Co/Ni ratio is due to variations in the Co content, which indicate slight fluctuations in the activity of CoS_2 during pyrite deposition (Herbert, 1987).

5.4. Chalcopyrite

Chalcopyrite is a minor phase in the main sphalerite–galena orebodies. It is fine- to medium-grained (≤ 1 mm) and occurs as interstitial disseminations or as patchy aggregates with mutual interference boundaries against the main sulphides. Chalcopyrite (Fig. 7a) is usually homogeneous, but in places contains very fine-grained, oriented laths of renierite or briartite (up to 20 µm long) and may itself occur as blebs in briartite. These exsolution intergrowths indicate cogenetic formation of chalcopyrite, briartite and renierite from a parent Cu–Ge–Fe–S solid solution. Chalcopyrite is partially replaced by galena and covellite (Fig. 7a) and deformation is indicated by grain fracturing and twin lamellae. It heals fractures in pyrite and appears to have been remobilised into intergranular areas of low stress during deformation.

The average chemical composition of chalcopyrite corresponds to a structural formula of $Cu_{1.01}Fe_{0.96}Ge_{0.01}S_2$. Apart from the occurrence of high values of Ge in chalcopyrite grains containing intergrowths of germanium sulphides, no other significant difference in the composition of chalcopyrite grains was observed. A maximum value of 0.04 wt.% V was measured in one sample from the No. 3/4 orebody, but the V content is generally negligible, along with that of As, Co and Ni. The Zn concentration in chalcopyrite is also very low and only amounts to an average of 0.05 wt.%.

Ge concentrations in chalcopyrite range from 0.19 to 0.63 wt.%, with an average of 0.31 wt.% Ge. Extremely high values of Ge are associated with high Zn and low Fe contents, indicating the occurrence of briartite intergrowths in chalcopyrite. Ge is known to substitute for Fe in chalcopyrite, resulting in an expansion of the chalcopyrite lattice, especially along the *c*-axis (Takeno, 1975). The coexistence of chalcopyrite and briartite indicates metastability due to cooling from a high temperature solid solution. According to Takeno (1975), the β-low temperature polymorph of chalcopyrite may contain up to 4 wt.% briartite in solid solution at 480 °C.

5.5. Germanium sulphides

Briartite [$Cu_2(Fe,Zn)GeS_4$] and renierite ($Cu_{3-x}Ge_xFeS_4$) are the two rare Ge-sulphides observed in the massive ores. Briartite is very fine-grained (20 to 90 μm) and occurs as rounded to oval grains enclosed in pyrite, galena or sphalerite (Fig. 7a, b). It also occurs as minute exsolution blebs in chalcopyrite and some briartite grains contain very fine-grained blebs of chalcopyrite. Briartite is greenish-grey to light grey in colour and weakly to distinctly anisotropic with brownish tints. Grains of briartite with inclusions of renierite are slightly darker and have a bluish tint, whereas homogeneous, inclusion-free grains are lighter with a greenish tint.

Just, like briartite, renierite is observable only on the microscopic scale. Renierite is homogeneous or inhomogeneous with lighter and darker areas due to compositional variations. It occurs as inclusions in briartite, chalcopyrite or sphalerite and may be replaced by galena (Fig. 7c, d). Inclusions of renierite in chalcopyrite and sphalerite form exsolution blebs up to 20 μm long. Renierite is distinguished by its beige colour and a distinct to strong anisotropy with yellowish brown to dark brown colours in some relatively coarse grains (up to 200 μm). The beige colour of renierite is similar to that of bornite, but unlike bornite it does not tarnish and it exhibits strong anisotropism.

5.6. Covellite and chalcocite

Covellite (CuS) and chalcocite (Cu_2S) are of secondary origin in the massive sulphide ores and occur in the cementation zone between the massive sulphide and the willemite ores. Fine-grained covellite flakes (≤ 0.1 mm) are typically intergrown with the second generation of galena around and within primary grains of sphalerite and pyrite. Covellite occurs in trace amounts and may contain relict inclusions of chalcopyrite, attesting to its formation through replacement of chalcopyrite. Chalcocite is less abundant than covellite and occurs in anhedral grains up to 0.1 mm across. In places it is intergrown with galena and replaces chalcopyrite as well as pyrite.

5.7. Silicate ore

The silicate ore at Kabwe is so-called because of the ubiquitous presence of willemite in the ore. The term silicate ore includes the predominantly willemite-rich ore in the oxidation zones around massive sulphide orebodies as well as mineralized jasperoid at the wall-rock contacts. The oxidation of the massive sulphide ores has in some cases resulted in ore zones composed entirely of silicate ore with or without remnants of sulphide bodies such as in some parts of the 5/6 orebody (between 850 and 1090 ft levels) and the No. 3/4 orebody (below the 1090 ft level). The No. 2 orebody is characterised by this typically Pb-poor and Fe-rich type of mineralization.

5.8. Willemite ore

The willemite-rich ore occurs mainly in the No. 2 orebody and in the oxidised zones of the Pb-rich orebodies (No. 5/6, No. 3/4 and No. 1). Some minor orebodies, such as the No. 2 H/W and the Foundry, are also characterised by this ore type. The ore consists mainly of willemite with minor smithsonite, cerussite, quartz, goethite and hematite. Relict cores of sphalerite and galena surrounded by smithsonite and cerussite are present where replacement is incomplete. Pyrite is commonly completely altered to goethite and hematite, which typically form a cellular-boxwork structure around the other secondary minerals and impart a red–brown colour to the ore. In addition, this ore type contains minor to trace amounts of quartz, covellite, pyromorphite, vanadinite, descloizite, mottramite, mimetite and dolomite. Only quartz shows evidence of grain fracturing.

Willemite (Zn_2SiO_4) forms massive aggregates and in places contains veins and vugs filled by later quartz. In hand specimen the colour of willemite is white, grey or brown. It shows no fluorescence in ultra-violet light, even on polished sections, indicating that it is relatively free of impurities. Two varieties of willemite are recognisable in thin section (Fig. 8a). One variety is relatively fine-grained (≤ 0.02 mm), equigranular and surrounded by a more tabular, coarser-grained (0.2 to 1.0 mm) variety. Fine-grained willemite is usually stained brown due to finely divided iron oxide inclusions, whereas coarse-grained willemite is colourless and free of inclusions. Coarse-grained willemite typically occurs in randomly oriented radial aggregates and also forms bands, 1 to 2 mm in width, along presumably pre-existing openings, indicating that it is younger. Prismatic crystals of willemite are also common in goethite-lined vugs or in druses within compact, massive willemite, consisting of interlocking hexagonal prisms with a granular or radiating texture.

Smithsonite ($ZnCO_3$) forms massive patchy aggregates of interlocking grains. It is commonly intergrown with willemite and occurs as disseminations in the latter mineral. Smithsonite replaces sphalerite (Fig. 6a, c, d) and it either replaces or is replaced by willemite. Anhedral masses of smithsonite typically contain inclusions

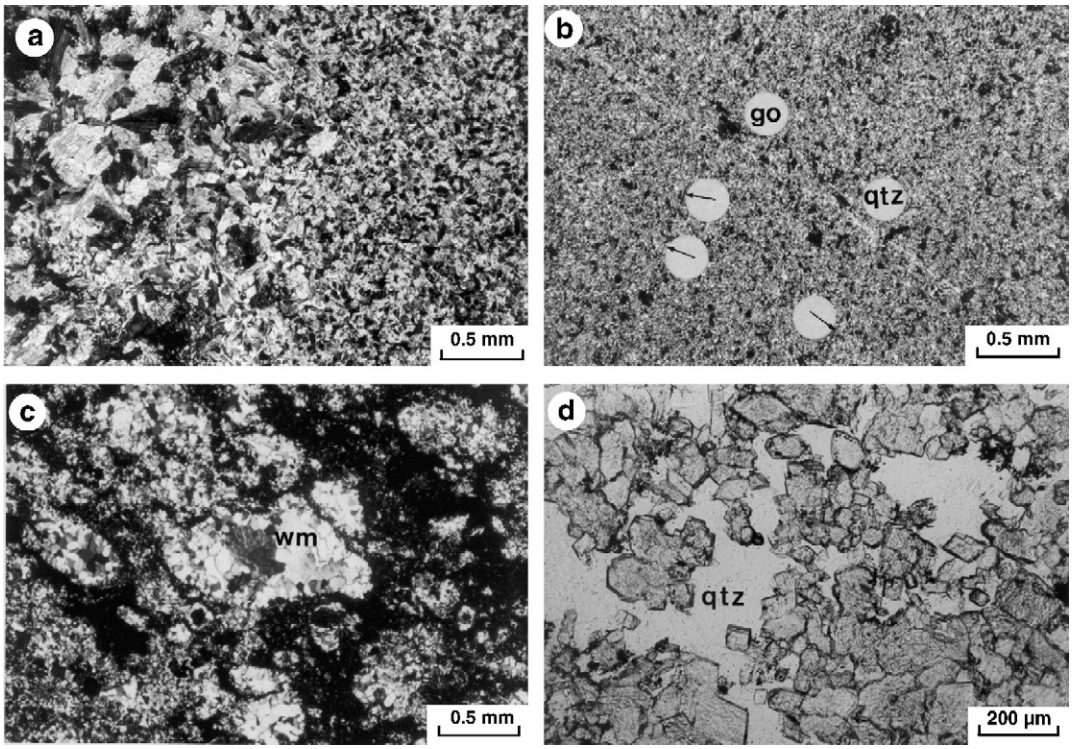

Fig. 8. Photomicrographs of silicate ore and wallrock dolomite. (a) Massive willemite ore with randomly oriented, tabular willemite adjacent to finer grained willemite, No. 3/4 orebody, 1090 ft level, crossed nicols; (b) Fine-grained jasperoid with disseminated goethite (go, black), prismatic grains of pyromorphite, descloizite and vanadinite (arrows, indistinguishable grey to black) and a quartz veinlet (qtz, white), No. 3/4 orebody, 1106 ft level; (c) Black jasperoid with quartz-lined vugs filled by willemite (wm) and quartz (grey and white pleochroism), No. 3/4 orebody, 1090 ft level, crossed nicols. (d) Silicified dolomite with grey recrystallized dolomite (rhombic) set in a white quartz matrix (qtz); 1 m from No. 5/6 orebody contact, 880 ft level.

of galena and covellite and fine-grained disseminations of goethite. Smithsonite is also intergrown with willemite and goethite in veinlets cutting across sphalerite grains. White cerussite ($PbCO_3$) occurs in massive aggregates and it is locally be rimmed by botryoidal smithsonite intergrown with willemite.

Quartz (SiO_2) occurs as interstitial grains as well as in veins and vugs in the willemite ore. Some quartz grains have secondary overgrowths of late quartz. In addition, the latest quartz generation occurs in cavities lined by goethite. Goethite (α-FeOOH) and hematite (Fe_2O_3) also occur in veinlets cutting across earlier mineral phases as well as in the more usual boxwork-structures after pyrite. In hand specimen goethite varies in colour from dark brown to light yellow and forms massive aggregates intergrown with hematite.

In polished section, goethite varies in colour from grey to dark grey. The dark grey variety often consists of cryptocrystalline masses, whereas grey goethite forms needle-like crystals. Dark grey cryptocrystalline goethite commonly occurs in innermost layers around pyrite, whereas grey goethite with intergrown hematite forms the outermost colloform bands. Hematite only occurs in minor amounts compared to goethite in the willemite ore.

Pyromorphite [$Pb_5(PO_4)_3Cl$], vanadinite [$Pb_5(VO_4)_3Cl$], descloizite [$Pb(Zn,Cu)OH{\cdot}VO_4$], mottramite [$Pb(Cu,Zn)OH{\cdot}VO_4$] and mimetite [$Pb_5(AsO_4)_3Cl$] occur in fibrous patches and as disseminations of fine-grained (≤ 0.05 mm), prismatic grains in willemite and goethite. Most of the prismatic minerals are coated by iron oxides. As a result, these minerals could only be distinguished by XRD analysis. Compositional variations among the phosphate, arsenate and vanadate minerals are indicated by the mutual occurrence of pyromorphite and mimetite, and of descloizite and mottramite, respectively. Arsenic may substitute for phosphorous in pyromorphite which forms a solid solution series with mimetite, whereas copper substitutes for Zn in descloizite which forms a solid solution series with mottramite.

Dolomite, $CaMg(CO_3)_2$ occurs in the silicate ore as relict grains partly replaced by willemite and quartz. It is

distinguished from smithsonite and cerussite by lower reflectance, a well developed cleavage and a lack of relict mineral inclusions.

5.9. Ferruginous jasper

Zones of ferruginous jasper occur within the orebodies and in the contact zones with wallrock dolomite. Ferruginous jasper is composed of very fine-grained quartz (≤0.01 mm) and its colour varies from black to grey to the more common red–brown varieties containing finely disseminated iron oxides. Textures vary from massive (Fig. 8b) to banded, and the jasperoid invariably contains microfractures of vein quartz. The banded texture is due to grain size variations of quartz. A nodular texture of quartz set in a dark matrix occurs in black jasperoid, which also contains white–pink quartz bands (≤1 cm). Late quartz and willemite commonly fill the vugs in the black jasper (Fig. 8c).

Variable amounts of disseminated hematite and goethite in jasperoid with cubic forms indicate that they are pseudomorphs after pyrite. Minor to trace willemite is disseminated in subidiomorphic grains characterised by hexagonal cross-sections, whereas smithsonite and cerussite commonly occur in veinlets together with colloform bands of hematite and goethite. Randomly oriented prismatic grains of vanadinite, pyromorphite and descloizite occur as disseminations and clusters associated with quartz in vugs. In addition, bands of chalcedony typically line the contact zone with wallrock dolomite, which is invariably silicified (Fig. 8d). Relict grains of dolomite may also occur in jasperoid, attesting to the formation of jasperoid by silicification of dolomite.

6. Sulphur isotopes

Sulphur isotope ratios ($\delta^{34}S_{CDT}$) of 56 sulphide mineral separates (Table 3) were determined in order to establish

Table 3
Sulphur isotope ratios (permil $\delta^{34}S_{CDT}$) of sulphide minerals from the massive, vein and disseminated types of mineralization

Sample no.	Location	Mineralization type	$\delta^{34}S_{pyrite}$	$\delta^{34}S_{sphalerite}$	$\delta^{34}S_{galena}$
302	1090 level, No. 3/4 orebody	Massive ore	−16.25	−17.54	−18.73
315	1106 level, No. 3/4 orebody	Massive ore	−14.88	−17.64	−18.72
312	1106 level, No. 3/4 orebody	Massive ore	−16.51	−18.01	−18.45
313	1106 level, No. 3/4 orebody	Massive ore	−15.01	−16.19	−18.44
OD4	Surface	Massive ore	−15.02	−16.15	−17.96
910/105	910 level, No. 1 orebody	Massive ore	−14.16	−15.87	−17.65
910/cd14	910 level, No. 1 orebody	Massive ore	−15.93	−16.64	−17.44
910/101	910 level, No. 1 orebody	Massive ore		−16.05	−17.40
316	1106 level, No. 3/4 orebody	Massive ore	−16.55	−17.37	
OD2	Surface	Massive ore	−16.99	−16.70	
910/102	910 level, No. 1 orebody	Massive ore		−16.36	−16.62
880/42d	880 level, No. 5/6 orebody	Massive ore	−16.30		
880/72b	880 level, No. 5/6 orebody	Massive ore	−16.15	−14.30	−16.10
880/6c	880 level, No. 5/6 orebody	Massive ore		−16.14	
910cd23	910 level, No. 5/6 orebody	Massive ore	−16.11		
OD8	850 level, No. 8 orebody	Massive ore		−15.20	
18E/6	525 level, No. 2 orebody	Massive ore	−13.40		
18E/7	525 level, No. 2 orebody	Massive ore	−12.65		
1250/24	1250 level, No. 2 orebody	Massive ore		−12.50	
1250/25	1250 level, No. 2 orebody	Massive ore	−10.20	−11.80	
18E/5	525 level, No. 2 orebody	Massive ore	−11.40	−10.80	
1050/1b	1050 level, No. 3/4 orebody	Vein	−11.40	−16.40	
1050/1a	1050 level, No. 3/4 orebody	Vein	−12.00	−13.10	
1250/83	1250 level, massive dolomite	Disseminated		−14.80	
1250/76	1250 level, massive dolomite	Disseminated		−14.40	
1250/72	1250 level, massive dolomite	Disseminated			−14.20
A2	50 level, carbonaceous dolomite	Disseminated		−14.10	
1250/75	1250 level, carbonaceous dolomite	Disseminated		−12.30	
850/14	850 level, schistose dolomite	Disseminated	−7.50		
850/8	851 level, schistose dolomite	Disseminated	−7.20		
850/17	852 level, schistose dolomite	Disseminated	−5.30		
850/13	853 level, schistose dolomite	Disseminated	−5.10		

the source of the sulphur and to test for equilibrium conditions in coexisting sulphides during and after sulphide deposition. The samples analysed include massive, vein and disseminated types of sulphides.

6.1. Massive sulphides

The sulphur isotopes ratios of 43 mineral separates of alena, sphalerite and pyrite from massive orebodies (Table 3) were determined from samples of varying metal ratios, including monomineralic phases in the case of sphalerite and pyrite. Occurrences of massive galena mineralization are, on the other hand, always accompanied by trace to minor sphalerite and pyrite. The distribution of sulphur isotope ratios within the main orebodies (Fig. 9) shows that sulphides from the Pb-rich orebodies (No. 1, No. 3/4 and No. 5/6) form a homogeneous group with negative δ^{34}S values ranging from −18.73‰ to −14.16‰. In contrast, sulphides from the Pb-poor No. 2 orebody are characterised by relatively heavier isotopic compositions (δ^{34}S from −13.4‰ to −10.2‰).

Galena, sphalerite and pyrite from the Pb-rich massive ores have mean δ^{34}S value of −17.75± 0.28‰ (1σ, n=10), −16.54±0.27‰ (n=13), and −15.82±0.25‰ (n=12), respectively. The narrow internal spreads for galena and sphalerite (<2‰), and pyrite (<3‰), indicate the general isotopic homogeneity of the sulphides within and between orebodies. Sphalerite from the monomineralic No. 8 orebody has an isotopic ratio (−15.20‰) that falls within the range of values from the Pb-rich orebodies. In contrast, sphalerite (δ^{34}S=−11.70±0.50‰, n=3) and pyrite (−11.91± 0.71‰, n=4) in the No. 2 orebody have relatively heavier sulphur isotope ratios. It was not possible to analyse galena from the No. 2 orebody as sufficiently pure material could not be recovered from this relatively Pb-poor orebody.

6.2. Vein sulphides

Sphalerite (δ^{34}S=−14.75±1.65‰, n=2) and pyrite (δ^{34}S=−11.70±0.30‰, n=2) samples from a 1 to 2 cm wide sulphide-willemite dolomite veinlet on the 1050 ft level in the vicinity of the No. 3/4 orebody have similar δ^{34}S values to the massive ores. The veinlet also contains microscopically visible galena, which could not be recovered in sufficient purity for isotopic analyses. The range in δ^{34}S values (−16.4 to −13.1‰) for vein

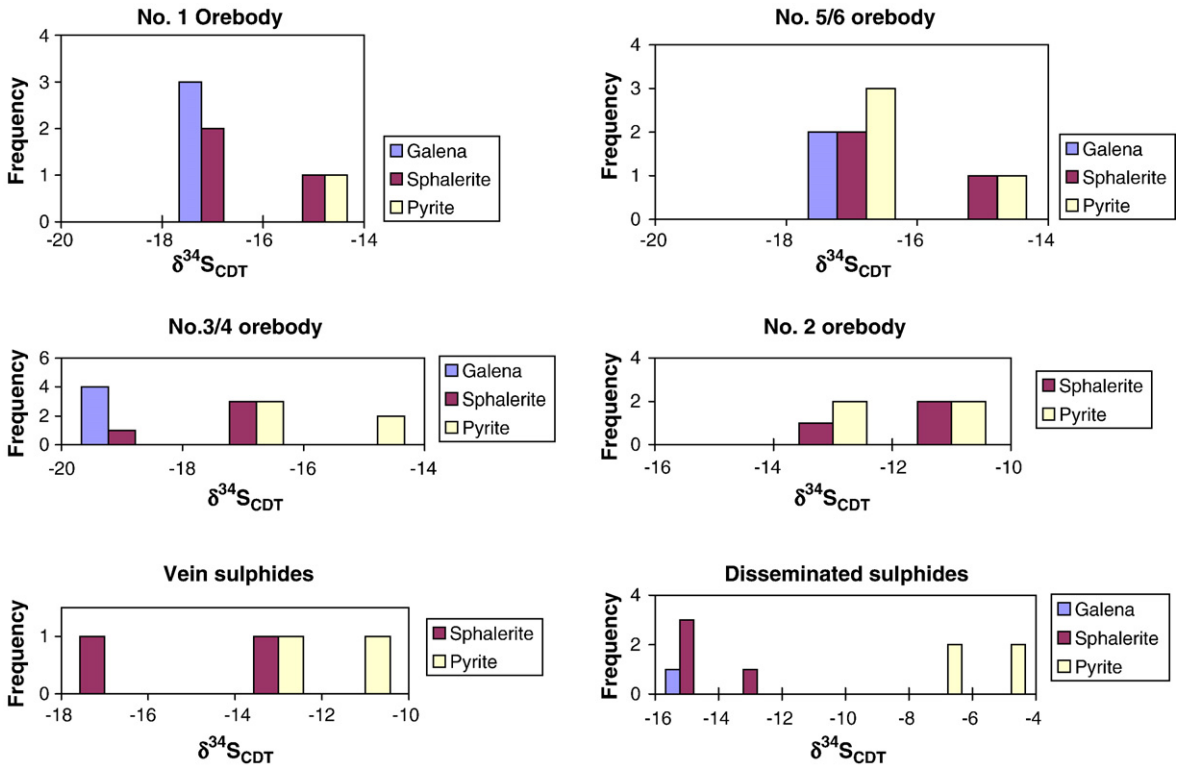

Fig. 9. Histogram plots of sulphur isotope ratios of sulphides from the No. 1, No. 3/4, No. 5/6, No. 2 orebodies and of vein and disseminated sulphides in massive, carbonaceous and schistose dolomite.

sphalerite overlaps with that of the massive Pb-rich and No. 8 orebodies (−18.01 to −14.30), and the No. 2 orebody (−12.50 to −10.80‰), respectively. The isotopic composition of vein pyrite is similar to that of pyrite in the No. 2 orebody, but it is significantly heavier than that of pyrite from the Pb-rich massive ores.

6.3. Disseminated sulphides

Disseminated sphalerite and galena occur in trace amounts in both massive and carbonaceous dolomite with galena rarer than the more generally widespread sphalerite. Galena occurs as isolated disseminations preferentially concentrated around sphalerite in an apparent replacement texture as observed in massive dolomite on the 1250 ft level (100 m north of the No. 2 orebody). The only ore concentrations of disseminated sphalerite occur at the Airfield orebody in carbonaceous dolomite.

The isotopic composition of disseminated galena (−14.20‰, $n=1$) is significantly heavier than that of galena from the Pb-rich massive ores (mean $\delta^{34}S=-17.75\pm0.28$‰, $n=10$). Disseminated sphalerite ($\delta^{34}S=-13.9\pm0.6$‰, $n=4$) has a comparable isotopic composition to that of vein sphalerite ($\delta^{34}S=-14.75\pm1.65$‰) and is only slightly lighter than No. 2 orebody sphalerite ($\delta^{34}S=-11.7\pm0.5$‰).

The range in isotopic composition of disseminated pyrite (−7.50‰ to −5.10‰, $n=4$) in the barren schistose dolomite represents the heaviest $\delta^{34}S$ ratios observed at Kabwe. The pyrite is isotopically homogeneous with a mean value of -6.28 ± 0.63‰ and it is significantly heavier than that of pyrite from the other rock types.

6.4. Sulphur isotope geothermometry

The application of stable isotope geothermometry is based on the equilibrium fractionation or partitioning of isotopes between two phases in an isotopic reaction (Kajiwara and Krouse, 1971; Ohmoto and Rye, 1979; O'Neil, 1986). The extent to which the partitioning of isotopes occurs is expressed as the fractionation factor α between a pair of chemical species. In general, the partition functions depend on the nature of the chemical bonds in a substance and on temperature, whereas the crystal structure of minerals has only a minor influence and the effect of pressure is negligible because the change in molar volumes of solids on isotopic substitution is small.

The isotopic enrichment in the Kabwe sulphides generally follows the equilibrium fractionation trend pyrite > sphalerite > galena, but a few samples show disequilibrium trends of sphalerite > pyrite and sphalerite > galena > pyrite.

6.4.1. Coexisting sulphide triplets

An approach towards equilibrium between coexisting pyrite, sphalerite and galena is shown by samples 313 and OD4 (Table 3), in which there are no isotopic reversals and the fractionations between sulphide pairs yield concordant isotopic temperatures in the range 227 to 356 °C. An isotopic temperature of 291 ± 35 °C is obtained from the graphical method of Javoy et al. (1970) by plotting the permil fractionation ($10^3\ln\alpha_{xy}$) of the mineral with the heaviest isotopes (in this case pyrite) against the fractionation coefficient A_{xy} of coexisting minerals.

6.4.2. Coexisting sulphide pairs

In an assemblage of sulphide triplets there is a possibility that one sulphide equilibrated with a second but not with the third sulphide due to differences in times of formation of the respective sulphides. In such cases equilibrium/disequilibrium relationships in mineral pairs are best evaluated by δ_x–δ_y plots (Gregory and Criss, 1986). Points of minerals which have equilibrated at the same temperature will lie along the same isotherm, but at widely different locations if they belong to systems with different bulk δ-values. Disequilibrium is indicated by non-parallelism of points to an isotherm.

6.4.3. Pyrite–galena

All the coexisting pyrite–galena pairs in samples ($n=8$) from the massive orebodies, except for sample 880/72b (Table 3), show the normal fractionation trend $\delta_{py}>\delta_{gn}$, where δ_{py} and δ_{gn} are the $\delta^{34}S$ ratios of pyrite and galena, respectively. The isotopic reversal in sample 880/72b is due to non-cogenetic crystallization of pyrite and galena as indicated by petrographic studies. The δ_{py}–δ_{gn} plot (Fig. 10a) shows a scatter of points with respect to isotherms, indicating non-parallelism of points and hence disequilibrium between pyrite and galena.

6.4.4. Sphalerite–galena

All of the ten coexisting sphalerite–galena pairs show a normal fractionation trend of $\delta_{sp}>\delta_{gn}$ (δ_{sp} being the $\delta^{34}S$ ratio of sphalerite). The permil fractionation between sphalerite and galena is, however, rather variable in these samples. Low fractionations, and consequently unusually high isotopic temperatures (significantly above 500 °C), are shown by some samples (Fig. 10b). The other samples have isotopic temperatures in the range 292 to 503 °C, but they do not show

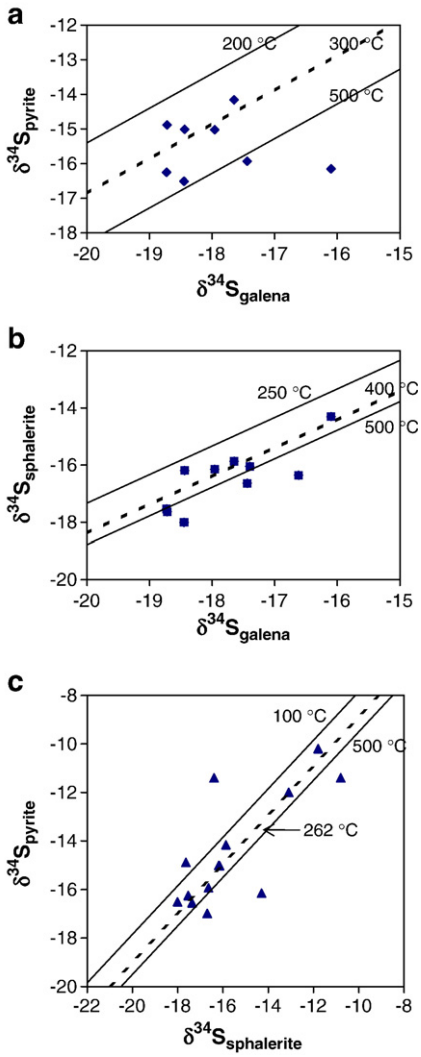

Fig. 10. δ_x–δ_y correlation plots for coexisting sulphide pairs with isotherms (°C). (a) $\delta^{34}S_{galena}$ versus $\delta^{34}S_{pyrite}$. (b) $\delta^{34}S_{galena}$ versus $\delta^{34}S_{sphalerite}$. (c) $\delta^{34}S_{sphalerite}$ versus $\delta^{34}S_{pyrite}$.

significant parallelism to the isotherms, indicating disequilibrium conditions during crystallization of galena. No mineralogical differences exist between these two sets of samples and the high temperatures could perhaps be due to disequilibrium during the formation of secondary galena, non-simultaneous deposition or the influence of a heating event, such as prograde metamorphism (O'Neil, 1986).

6.4.5. Pyrite–sphalerite

The normal fractionation trend $\delta_{py} > \delta_{sp}$ is shown by *all* but three of the 14 coexisting pyrite–sphalerite pairs. Two other samples (315 and 1050/1b; Table 3) have large fractionations that suggest disequilibrium crystallization. The indicated temperatures for these samples are too low to allow isotopic exchange and are typical of sulphide deposition as a result of biological activity (Nielsen, 1985). The rest of the pyrite–sphalerite pairs with isotopic temperatures in the range 143 to 372 °C are parallel to the isotherms (Fig. 10c). The δ_{py}–δ_{sp} values of these samples have a high correlation ($r = 0.989$) and define a regression line of slope 1.044 which is close to the ideal unit slope, indicating an approach towards equilibrium conditions during deposition. The estimated temperature of formation is 262 ± 29 °C for pairs with fractionations of < 1.34‰ (equivalent to the lower limit of 200 °C for the pyrite–sphalerite geothermometer).

7. Carbon and oxygen isotopes

The $\delta^{13}C_{PDB}$ and $\delta^{18}O_{SMOW}$ ratios of carbonaceous dolomite, schistose dolomite and massive dolomite are given in Table 4. Both the carbonaceous and massive dolomite types have similar isotopic ratios that are typical of marine carbonates (Fritz, 1976), with mean $\delta^{13}C_{PDB}$ and $\delta^{18}O_{SMOW}$ ratios of 2.89‰ and 27.68‰, respectively. The $\delta^{13}C$ values have a narrow spread (0.68‰) and fall within the well established ±3‰ variation of marine carbonate minerals relative to the PDB standard for most of the last 3.5 Ga (Ripperdan, 2001). The isotopically most enriched dolomite with a maximum $\delta^{13}C_{PDB}$ value of 3.18‰ probably reflects the seawater total dissolved carbon (TDC) during deposition of the Neoproterozoic Kabwe Dolomite Formation. The heavy $\delta^{13}C$ values could be due to a semiarid setting with very limited influence of plant-derived organic carbon.

Table 4
Oxygen ($\delta^{18}O_{SMOW}$) and carbon ($\delta^{13}C_{PDB}$) isotope ratios and silica content of dolomite samples from Kabwe

Sample no.	Rock type	$\delta^{18}O$ (‰)	$\delta^{13}C$ (‰)	SiO_2 (wt.%)
411	Massive dolomite	26.41	2.64	55.95
A1	Carbonaceous dolomite	26.81	3.08	1.75
405	Massive dolomite	26.95	2.50	17.94
1050/63	Carbonaceous dolomite	27.10	2.58	0.73
409	Massive dolomite	27.44	2.70	2.72
401	Massive dolomite	27.79	2.97	0.07
400	Massive dolomite	28.03	2.88	0.09
402	Massive dolomite	28.11	2.93	0.34
285	Massive dolomite	28.35	3.16	0.18
156	Schistose dolomite	28.65	0.87	13.55
278	Massive dolomite	28.68	3.18	0.05
235	Massive dolomite	28.81	3.15	0.05

The range in $\delta^{18}O$ values (2.40‰) is greater than that for the carbon isotopes, because of the relatively robust nature of $\delta^{13}C$ values, which are not fractionated as extensively by temperature as oxygen isotopes, and the extremely high elemental abundance of exchangeable oxygen relative to carbon in water (Scholle and Halley, 1985; Ripperdan, 2001).

The $\delta^{13}C_{PDB}$ and $\delta^{18}O_{SMOW}$ isotopes of the massive dolomite define an isotopic depletion trend (Fig. 11a) that correlates directly to the silica content of the whole-rock (Fig. 11b), indicating that the depletion trend in the host dolomite is due to wallrock silicification during the deposition of jasperoid from a SiO_2-rich fluid with high $\delta^{18}O$ ratios. The SiO_2 content varies from ≤0.05 wt.% in the least altered samples to a maximum of 55.95 wt.% in the most silicified sample (411), which is one meter from the orebody contact on the 880 ft level. Samples from the carbonaceous and the schistose dolomite types (Fig. 11) do not seem to be related to the isotopic depletion of $\delta^{13}C$ and $\delta^{18}O$, which is confined to silicified zones around the orebodies.

Electron microprobe analyses show that Mn and Fe are uniformly distributed as minor elements whose total concentration does not exceed 1 mol% $(Mn,Fe)CO_3$ in dolomite. Ba, Sr and S occur in concentrations below their respective detection limits, whereas measurable contents of Pb and Zn occur only in dolomite samples

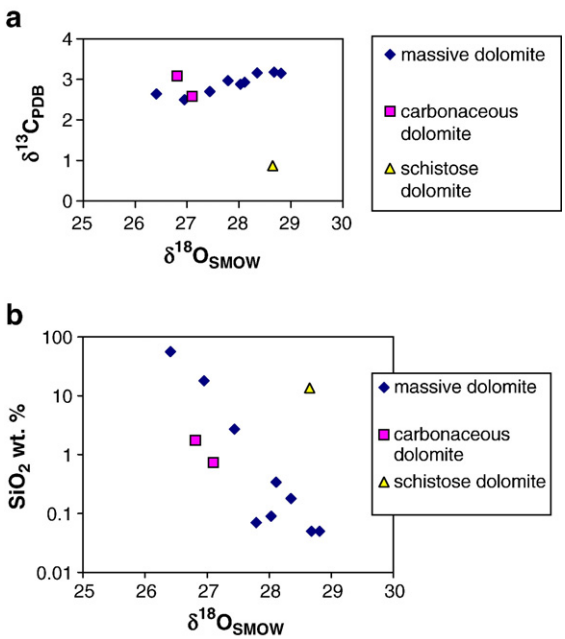

Fig. 11. (a) $\delta^{18}O_{SMOW}$ versus $\delta^{13}C_{PDB}$ in dolomite. Note the depletion trend indicated in massive dolomite samples. (b) Correlation of $\delta^{18}O_{SMOW}$ in dolomite versus SiO_2 content in whole rock.

marginal to the orebodies. Mn and Fe are relatively concentrated in fine-grained dolomite within 15 m of the orebodies with average values of 0.26 wt.% MnO and 0.22 wt.% FeO (n=31), respectively. Coarse-grained dolomite around the No. 8 orebody contains lower values of 0.11 and 0.10 wt.% MnO and FeO (n=5), respectively. The lowest values for MnO (0.06 wt.%) and FeO (0.02 wt.%) were found in a sample located 107 m north of the No. 2 orebody (n=9).

Whole rock chemical analyses show that Mn and Sr are uniformly distributed in massive dolomite with concentrations varying from 0.11 to 0.16 wt.% MnO and 80 to 90 ppm Sr, respectively. The lowest Mn (0.04 wt.% MnO) and Sr (10 ppm) values are associated with the silicified dolomite of the No. 5/6 orebody, which contains an average of 0.11 wt.% Mn and 64 ppm Sr, respectively (n=32).

8. Fluid inclusion studies

Sample materials for fluid inclusion studies included massive sulphide ores, vein mineralization, jasperoid and wallrock dolomite in which sphalerite, quartz and dolomite are the host minerals. The preliminary observations have shown that the inclusions occur along fracture planes in the host minerals and are therefore of secondary origin (Roedder, 1984). The fluid inclusions can be grouped into three types. Type 1 consists of liquid, vapour and solid crystals (L + V + S), Type 2 of liquid and vapour (L + V), whereas Type 3 is dominantly vapour-rich (V + L). The limited fluid inclusion data obtained so far is mostly from Type 1 and 2 fluid inclusions from a mineralized dolomite vein on the 1050 ft level near the No. 3/4 orebody and recrystallized dolomite at the margin of the No. 8 orebody. Type 3 inclusions were found mostly in sphalerite, whereas quartz in jasperoid contains Type 2 inclusions, but these have not been investigated due to their small size (≤1 μm).

8.1. Fluid inclusions with solid crystals

Type 1 fluid inclusions have mainly rounded, tabular and negative crystal forms (Fig. 12). Most of the solid inclusions probably consist of trapped crystals of dolomite since they are anisotropic, have a rhombic form and a birefringence similar to dolomite. Such fluid inclusions homogenise into the liquid state without dissolution of the trapped crystals upon heating to 500 °C. In some cases the solid crystals became slightly rounded as the corners were partially dissolved.

The Type 1 inclusions have homogenisation temperatures (T_h) in the range of 257 and 385 °C (Fig. 13).

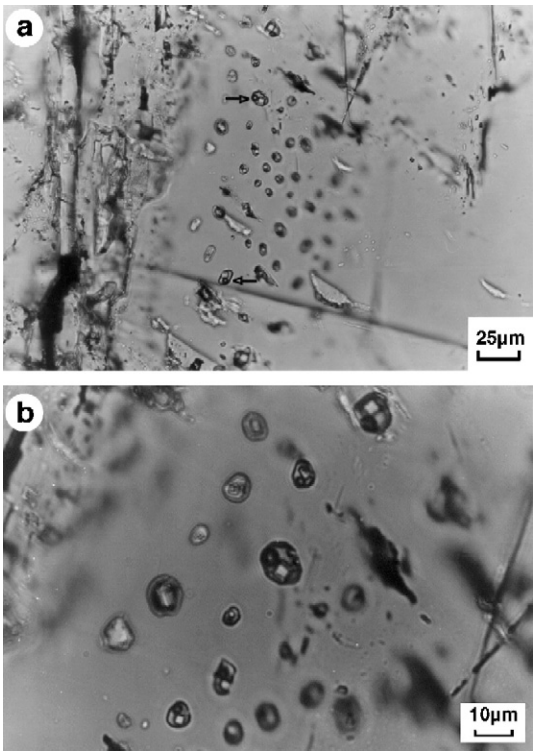

Fig. 12. Photomicrographs of fluid inclusions in dolomite. (a) Predominantly Type 1 (L + V + S) fluid inclusions along a fracture plane in dolomite, No. 3/4 orebody, 1050 ft level. (b) Detail of (a) showing solid inclusions and variation in fluid inclusion sizes from ≤3 to 10 µm.

Optical difficulties were encountered during freezing studies of these inclusions due to the high birefringence of the host dolomite. Two inclusions provided final melting temperatures (T_m) at −11 and −13.9 °C. According to the conversion formula of Bodnar (1993), the corresponding salinities are 15.0 and 17.7 eq. wt.% NaCl, respectively. In one instance, a Type 1 inclusion containing an isometric daughter crystal of halite, provided a dissolution temperature (T_s) of 195 °C and was completely homogenised into the liquid state at 257 °C. The dissolution temperature of the daughter crystal indicates a salinity of 31.6 eq. wt.% NaCl as determined from the equation of Bodnar and Vityk (1994). The estimated temperature of first melting (T_{fm}) obtained for the Type 1 fluid inclusions is in the range of −56 to −57 °C.

8.2. Liquid plus vapour inclusions

Type 2 fluid inclusions are irregular in form and have seemingly constant liquid:vapour ratios of about 90. Due to their small size (1 to 2 µm), only a small number provided homogenisation and freezing temperature data. These inclusions have homogenisation temperatures between 98 and 178 °C (Fig. 13), which are significantly lower than those obtained for the Type 1 inclusions. In one instance, a temperature of final melting (T_m) was determined at −7.8 °C, which corresponds to a salinity of 11.5 eq. wt.% NaCl.

8.3. Vapour-rich inclusions

It was not possible to obtain thermometric data in the Type 3 vapour-rich inclusions in sphalerite due to optical difficulties in observing the disappearance of the boundary between small amounts of liquid and the dark vapour phase. The inclusions have rounded shapes with a maximum size of 6 µm and they occur as trails of dark inclusions along fracture planes in sphalerite.

8.4. Fluid composition and pressure

An indication of the fluid composition may be obtained from the temperature of first visible appearance of liquid after complete melting. This temperature, which is also known as the temperature of first melting (T_{fm}), is close to the eutectic melting temperature, which is constant for a particular salt-water system (Shepherd et al., 1985). The estimated temperature of first melting obtained for the Type 1 fluid inclusions (−56 to −57 °C), is close to the −57 and −55 °C eutectic temperatures of the salt systems $NaCl–CaCl_2–MgCl_2–H_2O$ [Luzhnaya and Vereshtchetina (1946) in Mullis and Stalder (1987)] and $NaCl–CaCl_2–H_2O$ (Shepherd et al., 1985), indicating that the hydrothermal fluid contained several salts in solution.

The fluid inclusions with solid crystals probably formed during the recrystallization of the dolomite and the two-phase inclusions are presumed to have formed from later low temperature solutions probably associated with the thrust tectonics of the Lufilian orogeny. Alternatively, the low temperature inclusions could represent fluid mixing with meteoric water, but further

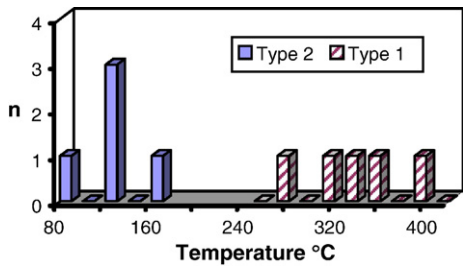

Fig. 13. Histogram of homogenisation temperatures for Type 1 and Type 2 fluid inclusions in host dolomite.

investigations are required to establish the paragenesis of the two types of fluid inclusions and the nature of the vapour-rich inclusions.

9. Discussion

The Kabwe Pb–Zn ores occur in the Kabwe Dolomite Formation, a carbonate platform sequence that forms part of the Neoproterozoic metasedimentary succession of the Lufilian fold belt in Zambia and the Democratic Republic of Congo (DRC). Sedimentation in the Lufilian fold belt occurred within an intracontinental rift setting characterised by clastic and playa sediments, dolomite carbonates, block faulting and bimodal volcanism (Raybould, 1978; Annels, 1984; Unrug, 1988, Porada, 1989; Kampunzu et al., 1991, 1993; Unrug, 1996). The sedimentary basin within the Kabwe–Sebembere area was characterised by a high heat flow as indicated by the occurrence of andesitic rocks and a tremolite schist of probable volcanic origin in the stratigraphic sequence (Cairney and Kerr, 1998; Sliwa and Podemski, in press).

The Kabwe orebodies are located along NE–SW trending faults that probably represent reactivated basement faults (De Swardt et al., 1965). The NE–SW fault system is cut-off by the N–S trending Mine Club fault zone, where the orebodies terminate, indicating that mineralization occurred before 528 Ma, which is the age of tectonic uplift in the Lusaka area (Barr et al., 1978). Roan Group sedimentation, which occurred between ca. 880 and 765 Ma (Armstrong et al., 1999; Key et al., 2001), provides a lower age limit for the epigenetic and structurally controlled orebodies.

Recent age dating research of MVT deposits has shown that such deposits formed mainly during contractional tectonic events and only a few formed during extensional tectonic events (Leach et al., 2001). The only age estimate for the Kabwe mineralization is the galena model isotopic age of 680 ± 13 Ma (Kamona et al., 1999). Mineralization could have occurred either after the extensional rift tectonic events associated with the Mwashya Group volcanism from 765 to 735 Ma (Key et al., 2001) or, during the contractional tectonic events associated with the early stages of the Lufilian orogeny of ca. 700 to 512 Ma (Cosi et al., 1992; Rainaud et al., 2002b).

The Kabwe deposit has been compared to the Berg Aukas-type mineralization in Namibia (Hughes et al., 1984; Hughes, 1987), where Frimmel et al. (1996) have distinguished between carbonate-hosted deposits related to extension and crustal thinning (Berg Aukas-type) and those related to continent collision and crustal thickening (Tsumeb-type). Duane and Saggerson (1995) and Kamona et al. (1999) have linked Cu–Pb–Zn mineralization in northern Namibia with Pan-African orogenesis. The recent preliminary Re–Os model age of 527 Ma for the Tsumeb deposit (Melcher et al., 2003) is in agreement with the galena model age of 530 ± 11 Ma for this deposit (Kamona et al., 1999), confirming that ore genesis is closely related to collisional tectonics and peak metamorphism in the Damaran orogen.

9.1. Sulphur and metal sources

Sulphur within the natural environment is ultimately either of igneous or seawater origin (Ohmoto and Rye, 1979). The isotopic compositions of the ore sulphides at Kabwe have homogeneous and negative δ^{34}S values with galena, sphalerite and pyrite averaging −17.43 ± 0.41‰, −15.23 ± 0.42‰ and −14.50 ± 0.50‰, respectively. Such negative δ^{34}S values with narrow ranges are indicative of sulphide accumulation in an open system with an infinite sulphate reservoir such as seawater sulphate in the pores of sediments accumulating in an anoxic environment (Schwarcz and Burnie, 1973; Goldhaber and Kaplan, 1974). Furthermore, the negative values are characteristic of sedimentary sulphides produced through bacterial reduction of seawater sulphate through a pyritization process in marine sediments leading to the accumulation of diagenetic sulphides with mean δ^{34}S values in the range −15‰ to −40‰ (Kaplan et al., 1963; Hartman and Nielsen, 1969; Goldhaber and Kaplan, 1974; Nielsen, 1985).

The amount of isotopic fractionation during sulphate reduction for the Kabwe sulphides is 33‰ as indicated by the difference between the isotopic composition of contemporaneous seawater sulphate during the late Precambrian, which had an average value of +17.5‰ for Copperbelt anhydrite and gypsum (Dechow and Jensen, 1965; Claypool et al., 1980), and the average δ^{34}S value of −15.8‰ for the ore sulphides. The fractionation factor of 33‰ is close to the 40‰ δ^{34}S average between seawater sulphate and sedimentary sulphides (Ohmoto, 1986).

The possible sulphur sources are the micaceous rocks of the Phyllite Formation, which probably contained the bulk of the diagenetic sulphides. Other rock units, including basal quartzite and basement schist, could also have provided some sulphur and associated metals during fluid circulation in deep rift faults within the Kabwe basin.

The source of the metals in the Kabwe orebodies is indicated by the isotopic signature of lead in galena to be the upper continental crust (Kamona et al., 1999). The

homogeneity of the lead isotopes coupled with the distinctly upper crustal signature, suggests prolonged hydrothermal circulation within a source reservoir in which significant radioactive decay had taken place to produce the high $^{207/204}$Pb and $^{208/204}$Pb ratios that plot above the Zartman and Doe (1981) average growth curve for the upper crust.

Possible source rocks for the metals include the basement rocks and disaggregated rocks of the basement that make up the sedimentary pile in the Kabwe basin. As indicated by the sulphur isotopes, the source of the Fe was mainly diagenetic pyrite in argillaceous sediments. In addition, a sedimentary rather than an igneous source for the Ge in the Kabwe deposit is more likely since obvious igneous rocks associated with the mineralization are lacking.

The isotopic depletion in ^{18}O in silicified zones around the orebodies indicates high temperature fluid–rock interaction during deposition of jasperoid. According to the fractionation factor of Land (1983) between dolomite and water, the calculated δ^{18}O value of the mineralizing fluid was in the range of 17‰ to 24‰ SMOW at temperatures between 257 and 385 °C. The high δ^{18}O values indicate that the ore fluid equilibrated with sediments is rich in δ^{18}O ratios such as shales, carbonates and cherts, which have typical values in the range +15‰ to +35‰ (Taylor, 1979).

9.2. Transport and deposition of metals

The available limited fluid inclusion data indicate at least two populations of fluid inclusions with homogenisation temperatures from 257 to 385 °C (Type 1 inclusions) and from 98 to 178 °C (Type 2). The Type 2 homogenisation temperatures are typical of MVT deposits, whose temperatures of deposition are low (75 to 200 °C) (Leach and Sangster, 1993), but the Type 1 values are much higher. However, high homogenisation temperatures in the range of 150 to 280 °C have recently been reported for MVT brines (Leach et al., 1997), indicating that the T_h values for the Kabwe ores are not that unusual. Comparable T_h values (190 to 266 °C) have also been recently obtained for the Khusib Springs deposit in the Otavi Mountain Land of Namibia (Chetty and Frimmel, 2000).

The salinity data indicate that some highly saline fluids may have been a source of the mineralization. Such high salinities (up to 31 eq. wt.% NaCl) could have been derived from extensive evaporation of seawater, the dissolution of evaporates or mixing between these end member water types (Hanor, 1996). The lower temperature and low salinity fluid represented by Type 2 inclusions indicate the involvement of more than one fluid type in the mineralization process. The preliminary data indicate possible mixing between fluids or, alternatively, the passage of post-mineralization fluids.

It is likely that the metals in the Kabwe ores were transported in solution as chloride complexes. As discussed by Hanor (1996) metal-rich brines form as a result of diagenetic destruction or alteration of metal-bearing solid phases in the presence of aqueous fluids of high salinity and low H_2S, and chloride complexing results in the preferential partitioning of the metal into the aqueous solution. There is no field or thermodynamic data to support the hypothesis that either organic complexes or reduced sulphur complexes are important in making metals soluble in typical basin waters (Hanor, 1996).

Ore deposition could have taken place as a result of a pH change, dilution or cooling (Barnes, 1979). In a carbonate environment, such as that at Kabwe, sulphide deposition from chloride complexed metals in the presence of H_2S is enhanced by reaction with carbonate rocks, which results in increased pH. Dilution by circulating meteoric waters or by addition of Cl ion-pairing cations like Ca^{2+} and Mg^{2+} from the dissolution of dolomite would result in decreased chloride concentrations, promoting further sulphide deposition.

Sulphide deposition at Kabwe was partly preceded by deposition of silica to form jasperoid through replacement of dolomite. The deposition of silica could have been promoted by metasomatic reaction of silicic acid in the ore solution with the carbonate host rocks (Barth, 1989). It is possible that the first generation of willemite observed in jasperoid formed during this phase of wallrock alteration from a silica- and iron-rich hydrothermal fluid as suggested by Hitzman et al. (2003) and Brugger et al. (2003). A hypogene origin for willemite is suggested by Sweeney et al. (1991) for the non-sulphide Star Zinc willemite deposit near Lusaka which contains primary two-phase (liquid + vapour) fluid inclusions with homogenisation temperatures in the range 150 to 250 °C and salinities between 5 and 22 eq. wt.% NaCl.

9.3. Post-mineralization events

The ore sulphides show evidence of recrystallization and deformation, such as bent cleavages, grain fracturing and remobilisation into intragranular zones of low stress. The mineral textures suggest that the ores experienced a phase of low grade metamorphism, possibly during the major event of the Lufilian orogeny estimated at ca. 550 Ma (Porada and Berhorst, 2000). It is

therefore possible that the isotopic model temperatures shown by the sulphide pairs in the range 260 to 377 °C may reflect the effects of the greenschist facies metamorphism associated with the Lufilian orogeny.

Progressive metamorphism could also explain disequilibrium in some sulphide pairs which show closed system behaviour as indicated by non-parallelism of these pairs to isotherms. However, due to the low metamorphic grade in the region (greenschist facies), it is more likely that disequilibrium is a result of the late paragenetic position of primary galena and of secondary processes associated with the oxidation of the sulphide ores as indicated by the formation of secondary galena in the cementation zone.

The primary sulphide minerals have been invariably altered during oxidation to produce the numerous secondary minerals found at Kabwe. The oxidation of the sulphides persists down to the deepest mining level (1550 ft) due to exposure of the orebodies to oxygenated ground waters along orebody contacts and fractures within the orebodies. Apart from phosphorous and vanadium, the sources of the elements that make up the secondary arsenates, oxides, carbonates, silicates, and sulphides, are the major and trace elements in the primary minerals themselves.

Fossil mammalian bones found in caves within the host dolomite are the source of the phosphorous in the oxidised zones of the orebodies (Mennell and Chubb, 1907; Spencer, 1908; Zealley, 1912). The source of vanadium, on the other hand, is not so evident, because primary vanadium bearing minerals have not been identified in the Kabwe ores so far. However, the geochemical distribution of vanadium in the orebodies suggests that it was derived externally and introduced into the oxidation zone by circulating meteoric waters. According to Skerl (1934) and Taylor (1954), vanadium was originally contained in micaceous country rocks of the Phyllite Formation, which is now partly removed by erosion.

Some of the silica that occurs mainly as vug quartz and chalcedony is also of secondary origin and was introduced into the oxidation zone by circulating ground waters (Taylor, 1958). The interaction of the silica with sphalerite during oxidation accounts for the abundance of coarse-grained willemite in pre-existing openings within the oxidation zone. Massive, finer grained willemite with iron-oxide inclusions could have formed during silicification of the wallrock dolomite at temperatures >150 °C under oxidizing conditions (Brugger et al., 2003), and would thus be hypogene. Alternatively, it could have formed during in situ oxidation of the primary sulphide ore and would therefore be supergene. The in situ oxidation of sphalerite to form willemite is considered more likely as indicated by the association of willemite with other secondary minerals such as smithsonite, cerussite, quartz, goethite and hematite and by the occurrence of relict cores of sphalerite and galena surrounded by smithsonite and cerussite in the silicate ore. In addition, only single-phase inclusions have been found in willemite from Kabwe (Groves et al., 2003).

9.4. Ore genesis

Various theories of ore genesis have been put forward to explain the formation of the Kabwe orebodies. Taylor (1954) proposed that the orebodies are a result of magmatic–hydrothermal activity. However, although the formation temperatures and pipe-like orebody morphology are similar to the high temperature carbonate replacement deposits of the Leadville-type (Megaw et al., 1988; Thompson and Beaty, 1990), igneous rocks directly associated with the mineralization are lacking and an igneous component is not supported by the isotopic evidence. Similarly, there is a lack of supporting evidence for the prior existence of proto-volcanogenic ores, from which the metals could have been mobilised (Sweeney et al., 1990). The only stratiform mineralization types in the area are Cu deposits in quartzite and Cu–Zn deposits of probable volcanogenic origin in tremolite schist (Cairney and Kerr, 1998), and both these deposit types lack Pb.

A karstic origin for the deposit (Sweeney and Binda, 1989; Samama et al., in press) is precluded by the high salinities of the ore fluid and the high temperatures of ore deposition. Furthermore, internal sediments typical of intra-karst sedimentation (Bernard, 1973) are lacking. Mobilisation of metals from sediments of the dolomite units (Kortman, 1972) is unlikely as the dolomite acted as a metal recipient rather than as a source of metals. The trace element and sulphur isotopic compositions of the disseminated sulphides in the dolomites are indistinguishable from the massive sulphide ores, suggesting that they represent a primary dispersion halo introduced epigenetically at the same time as the massive ores in dolomite.

Hughes et al. (1984) and Hughes (1987) favour accumulation of metals in ore fluids as a result of basin dewatering, but the mechanism of dewatering is not indicated. In this regard, Kortman (1972) suggested that the expulsion of metal-rich connate waters could be connected with the deformation of the sediments, whereas Unrug (1988) considers that the dewatering pulses were driven by metamorphism.

The processes of ore formation at Kabwe are related to the tectonic setting of the deposit in a continental rift environment with a high heat flow as indicated by minor extrusive rocks in the stratigraphic sequence. It is envisaged that the bulk of the metals were obtained by diagenetic destruction of alumino-silicates and pyrite in argillaceous rocks of the Phyllite Formation. Further hydrothermal leaching of metals could also have taken place during the volcanism associated with the Mwashia volcanics at 765 and 735 Ma (Key et al., 2001).

An upper continental setting is justified by the lead isotope data, which indicate that the source reservoir was a homogeneous region of the upper crust rich in uranogenic and thorogenic lead (Kamona et al., 1999). The sulphur as well as oxygen isotopes indicate that the source reservoir was sedimentary. Homogenisation of the lead and sulphur isotopes appears to have been achieved through prolonged residence time in an aquifer and by fluid circulation through large volumes of rock. The aquifer was probably the Arkose–Quartzite Formation that forms the base of the metasedimentary cover. Reactivated rift faults probably provided the necessary conduits for fluid migration upwards, under pressure, into fractured zones within dolomite.

10. Conclusions

Stable and radiogenic isotope and preliminary fluid inclusion data indicate that the Kabwe deposit formed from highly saline, high temperature fluids derived from formation waters that had equilibrated with sedimentary rocks within a continental rift environment. Fluid flow and ore deposition within the host dolomite were structurally controlled, indicating that mineralization of the Kabwe type is likely to be found in fractured zones within carbonates of the Kabwe Dolomite Formation.

The occurrence of the faults and a high geothermal gradient in a continental rift zone appears to have provided the necessary conditions for fluid circulation and mineralization in faulted zones of the dolomite. Wallrock alteration is indicated by silicification and the isotopic depletion in $\delta^{18}O$ values around the orebodies, but the isotopic depletion is confined to silicified zones in the immediate neighbourhood of the orebodies and is therefore of limited use as an exploration guide. Similarly, apart from Zn, most elements associated with the mineralization are confined to the orebodies and are not widely dispersed within the host dolomite. Zn appears to be more widely dispersed than other elements and could therefore be used as an exploration guide in conjunction with structural mapping to delineate faulted zones in dolomite.

In addition, the previously mined waste dumps at Kabwe can be re-examined as potential sources of Ge, Ga and In, whereas the smaller mineral occurrences in the Kabwe region are potential sources of non-sulphide zinc.

Acknowledgements

This paper is a contribution to IGCP 450 and is dedicated to the memory of the late Henri Kampunzu who handled the original editorial work. The basic research work was financed by DAAD and the University of Zambia. ZCCM (Kabwe Division) provided invaluable support. Stable isotope analyses were made possible by the Scottish Universities Research and Reactor Centre in Glasgow, Scotland The assistance of colleagues at RWTH Aachen with sample preparation and analysis is gratefully acknowledged. The manuscript benefited greatly from critical comments by Prof. Hartwig Frimmel and Prof. Philippe Muchez.

References

Annels, A.E., 1984. The geotectonic environment of Zambian copper–cobalt mineralisation. Journal of the Geological Society (London) 141, 279–289.

Armstrong, R.A., Robb, L.J., Master, S., Kruger, F.J., Mumba, P.A.C.C., 1999. New U–Pb age constraints on the Katangan Sequence, Central African Copperbelt. Journal of African Earth Sciences 28 (4A), 6–7.

Arthurs, J.W., Newman, D., Smith, A.G., 1995. Geology of the Chipembi area: explanation of degree sheet 1438, SE quarter. Geological Survey of Zambia, Report 58, 37.

Bancroft, J.A., 1961. The Rhodesia Broken Hill Development Company Limited. In: Guernsey, T.D. (Ed.), Mining in Northern Rhodesia: Period of Achievement and Reward, From 1931. British South Africa Company, pp. 112–122.

Barnes, H.L., 1979. Solubilities of ore minerals, In: Barnes, H.L. (Ed.), Geochemistry of Hydrothermal Ore Deposits, 2nd ed. Wiley-Interscience, New York, pp. 404–460.

Barr, M.W.C., Cahen, L., Ledent, D., 1978. Geochronology of syntectonic granites from Central Zambia: Lusaka granite and granite NE of Rufunsa. Annales de la Société Géologique de Belgique 100, 47–54.

Barth, A., 1989. Cause and efficiency of geochemical barriers related to the origin of hydrothermal–metasomatic zinc sulphide mineralisation in carbonate host rocks. Zeitschrift für Angewandte Geologie 35, 208–216.

Bernard, A.J., 1973. Metallogenic processes of intrakarstic sedimentation. In: Amstutz, G.C., Bernard, A.J. (Eds.), Ores in Sediments. Springer-Verlag, Berlin, pp. 43–57.

Bodnar, R.J., 1993. Revised equation and table for determining the freezing point depression for of H_2O–NaCl solutions. Geochimica et Cosmochimica Acta 57, 683–684.

Bodnar, R.J., Vityk, M.O., 1994. Interpretation of microthermometric data for H_2O–NaCl fluid inclusions. In: de Vivo, B., Frezzotti, M.L. (Eds.), Fluid Inclusions in Minerals: Methods and Applications. Virginia Polytechnic Institute and State University, pp. 117–130.

Braithwaite, R.S.W., 1988. Spencerite from Kabwe, Zambia, and the infrared spectroscopy of the Kabwe zinc phosphates. Mineralogical Magazine 52, 126–129.

Brugger, J., McPhail, D.C., Wallace, M., Waters, J., 2003. Formation of willemite in hydrothermal environments. Economic Geology 98, 819–835.

Cahen, L., Snelling, N.J., Delhal, J., Vail, J.R., 1984. The Geochronology and Evolution of Africa. Clarendon Press, Oxford. 512 pp.

Cairney, T., Kerr, C.D., 1998. The geology of the Kabwe area: explanation of degree sheet 1428, NW quarter. Geological Survey of Zambia, Report 47, 40.

Chetty, D., Frimmel, H.E., 2000. The role of evaporates in the genesis of base metal sulphide mineralisation in the Northern Platform of the Pan-African Damara Belt, Namibia: geochemical and fluid inclusion evidence from carbonate wall rock alteration. Mineralium Deposita 35, 364–376.

Claypool, G.E., Holser, W.T., Kaplan, I.R., Sakai, H., Zak, I., 1980. The age curves of sulphur and oxygen isotopes in marine sulphate and their mutual interpretations. Chemical Geology 28, 199–260.

Colby, J.W., 1968. Quantitative microprobe analysis of thin insulating films. Advances in X-ray Analysis 11, 287–305.

Coles, J., 1959. The geology and mineralisation of Broken Hill, northern Rhodesia. Unpublished Ph.D. thesis, Royal School of Mines, London.

Cosi, M., De Bonis, A., Gosso, G., Hunziker, J., Martinotti, G., Moratto, S., Robert, J.P., Ruhlman, F., 1992. Late Precambrian thrust tectonics, high pressure metamorphism and uranium mineralisation in the Domes area, Lufilian Arc, northwestern Zambia. Precambrian Research 58, 215–240.

Dawson, A.R., in press. Final report on Sebembere EL 34. Mokambo Development Company.

De Swardt, A.M.J., Garrard, P., Simpson, J.G., 1965. Major zones of transcurrent dislocation and superposition of orogenic belts in parts of Central Africa. Geological Society of America Bulletin 76, 89–102.

Dechow, E., Jensen, M.L., 1965. Sulphur isotopes of some Central African sulphide deposits. Economic Geology 60, 894–941.

Duane, M.J., Saggerson, E.P., 1995. Brine expulsion, fluid transport and metallization spanning 2.0 Gyr in basins of southern and central Africa. Basin Research 7, 97–108.

Frimmel, H.E., Deane, J.G., Chadwick, P.J., 1996. Pan-African tectonism and the genesis of base metal sulfide deposits in the northern foreland of the Damara orogen, Namibia. In: Sangster, D.F. (Ed.), Carbonate-Hosted Lead–Zinc Deposits. Special Publication, vol. 4. Society of Economic Geologists, pp. 204–217.

Fritz, P., 1976. Oxygen and carbon isotopes in ore deposits in sedimentary rocks. In: Wolf, K.H. (Ed.), Handbook of Stratabound and Stratiform Ore Deposits, vol. 2. Elsevier, Amsterdam, pp. 191–217.

Gair, H.S., 1960. The Karroo system of the western end of the Luano Valley. Geological Survey of Northern Rhodesia, Report, vol. 6. 40 pp.

Goldhaber, M.B., Kaplan, I.R., 1974. The sulphur cycle. In: Goldberg, E.D. (Ed.), The Sea. Wiley-Interscience, New York, pp. 569–655.

Gregory, R.T., Criss, R.E., 1986. Isotopic exchange in open and closed systems. In: Valley, J.W., Taylor Jr, H.P., O'Neil, J.R. (Eds.), Stable Isotopes in High Temperature Geological Processes. Reviews in Mineralogy, vol. 16. Mineralogical Society of America, pp. 91–127.

Groves, I.M., Carman, C.E., Dunlap, W.J., 2003. Geology of the Beltana willemite deposit, Flinders Ranges, South Australia. Economic Geology 98, 797–818.

Guernsey, T.D., 1953. Summary of early prospecting in northern Rhodesia. Transactions of the Institution of Mining and Metallurgy 63, 1–8.

Haldane, R., in press-a. Kabwe mine compilation of geological work in the Airfield area. ZCCM (Operations Centre) Technical Services, Kalulushi.

Haldane, R., in press-b. Kabwe mine compilation of geological work in the Foundry area. ZCCM (Operations Centre) Technical Services, Kalulushi.

Hanor, J.S., 1996. Controls on the solubilization of basinal brines. Economic Geology Special Publication 4, 483–500.

Hartman, M., Nielsen, H., 1969. δ^{34}S-Werte in rezenten Meeressedimenten und ihre Deutung am Beispiel einiger Sedimentprofile aus der westlichen Ostsee. Geologische Rundschau 58, 621–655.

Herbert, H.K., 1987. Minor element compositions of sphalerite and pyrite as petrogenetic indicators. Proceedings International Pacific Rim Congress 1987, Gold Coast, Queensland. Australian Institute of Mining and Metallurgy, pp. 831–841.

Hitzman, M.W., Reynolds, N.A., Sangster, D.F., 2003. Classification, genesis, and exploration guides for nonsulfide zinc deposits. Economic Geology 98, 685–714.

Hubbard, G.D., 1913. Rare minerals at Broken Hill, Rhodesia. Engineering and Mining Journal 95, 1297–1298.

Hughes, M.J., 1987. The Tsumeb ore body, Namibia, and related dolostone-hosted base metal deposits of Central Africa. Ph.D. thesis, University of the Witwatersrand, Johannesburg, South Africa. 448 pp.

Hughes, M.J., Welke, H.J., Allsop, H.L., 1984. Lead isotopic studies of some Late Proterozoic stratabound ores of Central Africa. Precambrian Research 25, 137–139.

Javoy, M., Fourcade, S., Allegre, C.J., 1970. Graphical method for examination of $^{18}O/^{16}O$ fractionations in silicate rocks. Earth and Planetary Science Letters 10, 12–16.

Kajiwara, Y., Krouse, H.R., 1971. Sulphur isotopic partitioning in metallic sulphide systems. Canadian Journal of Earth Science 8, 1397–1408.

Kamona, A.F., 1993. The carbonate-hosted Kabwe Pb–Zn deposit, Central Zambia. PhD dissertation, Technical University of Aachen, Aachen, Germany. 207 pp.

Kamona, F., Friedrich, G., 1994. Die Blei-Zink Lagerstätte Kabwe in Zentral Sambia. Erzmetall 47, 34–44.

Kamona, F., Friedrich, G.H., Sweeney, M.A., 1990. The Kabwe Pb–Zn deposit in Central Zambia. In: Rocci, G., Deschamps, M. (Coordinators); Recent Data in African Earth Sciences. CIFEG Occasional Publication 1990/22, Nancy, 325–327.

Kamona, F., Friedrich, G.H., Le Roux, A., 1991a. Primary and secondary minerals from the Kabwe Zn–Pb deposit, Zambia. Zambian Journal of Applied Earth Sciences 5, 51–56.

Kamona, F., Friedrich, G.H., Sweeney, M.A., Fallick, A.E., 1991b. Stable isotopes of the Kabwe lead–zinc deposit. In: Pagel, M., Leroy, J.L. (Eds.), Source, Transport and Deposition of Metals. Balkema, Rotterdam, pp. 313–316.

Kamona, A.F., Lévêque, J., Friedrich, G., Haack, U., 1999. Lead isotopes of the carbonate-hosted Kabwe, Tsumeb, and Kipushi Pb–Zn–Cu sulphide deposits in relation to Pan African orogenesis in the Damaran–Lufilian fold belt of Central Africa. Mineralium Deposita 34, 273–283.

Kampunzu, A.B., Kapenda, D., Manteka, B., 1991. Basic magmatism and geotectonic evolution of Pan-African belts in Africa: evidence from the Katangan and West Congolian segments. Tectonophysics 190, 363–371.

Kampunzu, A.B., Kanika, M., Kapenda, D., Tshimanga, K., 1993. Geochemistry and geotectonic setting of Late Proterozoic Katangan basic rocks from Kibambale in central Shaba (Zaire). Geologische Rundschau 82, 619–630.

Kaplan, I.R., Emery, K.O., Rittenberg, S.C., 1963. The distribution and isotopic abundance of sulphur in recent marine sediments off

southern California. Geochimica et Cosmochimica Acta 27, 297–331.

Key, R.M., Liyungu, A.K., Njamu, F.M., Somwe, V., Banda, J., Mosley, P.N., Armstrong, R.A., 2001. The western arm of the Lufilian Arc in NW Zambia and its potential for copper mineralization. Journal of African Earth Sciences 33, 503–528.

Kortman, C.R., 1972. The geology of the Zambia Broken Hill Mine, Kabwe. Geologie en Mijnbouw 51, 347–356.

Land, L.S., 1983. The application of stable isotopes to studies of the origin of dolomite and to problems of diagenesis of clastic sediments. In: Arthur, M.A., Anderson, T.F., Kaplan, I.R., Veizer, J., Land, L.S. (Eds.), Stable Isotopes in Sedimentary Geology-SEPM Short Course, vol. 10, pp. 4-1–4-22.

Leach, D.L., Sangster, D.F., 1993. Mississippi Valley-type lead–zinc deposits. In: Kirkham, R.V., Sinclair, W.D., Thorpe, R.I., Duke, J.M. (Eds.), Mineral Deposit Modeling. Special Paper, vol. 40. Geological Association of Canada, pp. 289–314.

Leach, D.L., Apodaca, L.E., Repetski, J.E., Powell, J.W., Rowan, E.L., 1997. Evidence for hot Mississippi Valley-type brines in the Reelfoot Rift Complex, south-central United States, in Late Pennsylvanian–Early Permian. U.S. Geological Survey Professional Paper 1577, 36.

Leach, D.L., Bradley, D., Lewchuk, M.T., Symons, D.T.A., de Marsily, G., 2001. Mississippi Valley-type lead–zinc deposits through geological time: implications from recent age-dating research. Mineralium Deposita 36, 711–740.

McCrea, J.M., 1950. On the isotopic chemistry of carbonates and a paleotemperature scale. Journal of Chemical Physics 18, 849–857.

Megaw, P.K.M., Ruiz, J., Titley, S.R., 1988. High-temperature, carbonate-hosted Ag–Pb–Zn(Cu) deposits of northern Mexico. Economic Geology 83, 1856–1885.

Melcher, F., Oberthur, T., Vetter, U., Gross, C., Vollbrecht, A., Brauns, M., Haack, U., 2003. Enrichment of germanium in base metal mineralization of the Otavi Mountain Land, Namibia. In: Cailteux, J.L.H. (Ed.), Proterozoic Sediment-Hosted Base Metal Deposits of Western Gondwana, Lubumbashi 2003, pp. 156–159. Extended abstracts.

Melcher, F., Oberthur, T., Rammlmair, D., 2006. Geochemical and mineralogical distribution of germanium in the Khusib Springs Cu–Zn–Pb–Ag sulfide deposit, Otavi Mountain Land, Namibia. Ore Geology Reviews 28, 32–56.

Mennell, F.P., 1920a. Rare zinc–copper minerals from the Rhodesia Broken Hill mine, northern Rhodesia. Mineralogical Magazine 19, 69–72.

Mennell, F.P., in press. Estimate of zinc ore reserves. Rhodesia Broken Hill Development Company Limited.

Mennell, F.P., Chubb, E.C., 1907. On an African occurrence of fossil mammalian associated with stone implements. Geological Magazine 43, 443–448.

Moore, T.A., 1964. The geology of the Chisamba area: explanation of degree sheet 1428, SW quarter. Geological Survey of Zambia, Report 5, 32.

Mullis, J., Stalder, H.A., 1987. Salt-poor and salt-rich fluid inclusions in quartz from two boreholes in northern Switzerland. Chemical Geology 61, 263–272.

Nielsen, H., 1985. Sulphur isotope ratios in stratabound mineralizations in Central Europe. Geologisches Jahrbuch D70, 225–262.

Notebaart, C.W., Korowski, S.P., 1980. The Broken Hill Mine, Zambia. Mineralogical Record 11, 339–348.

Ohmoto, H., 1986. Stable isotope geochemistry of ore deposits. In: Valley, J.W., Taylor, H.P., O'Neil, J.R. (Eds.), Stable Isotopes in High Temperature Geological Processes. Reviews in Mineralogy, vol. 16. Mineralogical Society of America, pp. 491–559.

Ohmoto, H., Rye, R.O., 1979. Isotopes of sulphur and carbon, In: Barnes, H.L. (Ed.), Geochemistry of Hydrothermal Ore Deposits, 2nd ed. Wiley-Interscience, New York, pp. 509–567.

O'Neil, J.R., 1986. Theoretical and experimental aspects of isotopic fractionation. In: Valley, J.W., Taylor, H.P., O'Neil, J.R. (Eds.), Stable Isotopes in High Temperature Geological Processes. Reviews in Mineralogy, vol. 16. Mineralogical Society of America, pp. 1–40.

Pelletier, R.A., 1929. The zinc, lead and vanadium deposits of Broken Hill, northern Rhodesia. XV International Geological Congress, South Africa, Guide Book, Excursion, vol. C22, pp. 13–16.

Porada, H., 1989. Pan-African rifting and orogenesis in southern to equatorial Africa and eastern Brazil. Precambrian Research 44, 103–136.

Porada, H., Berhorst, V., 2000. Towards a new understanding of the Neoproterozoic–Early Palaeozoic Lufilian and northern Zambezi belts in Zambia and the Democratic Republic of Congo. Journal of African Earth Sciences 30, 727–771.

Rainaud, C., Armstrong, R.A., Master, S., Robb, L.J., Mumba, P.A.C.C., 2002a. Contributions to the geology and mineralization of the Central African Copperbelt: I. Nature and geochronology of the Pre-Katangan basement. 11th IAGOD Quadrennial Symposium and Geocongress, Windhoek, Namibia. Geological Survey of Namibia. CD-ROM.

Rainaud, C., Master, S., Armstrong, R.A., Phillips, D., Robb, L.J., 2002b. Contributions to the geology and mineralization of the Central African Copperbelt: IV. Monazite U–Pb dating and ^{40}Ar–^{39}Ar thermochronology of metamorphic events during the Lufilian orogeny. 11th IAGOD Quadrennial Symposium and Geocongress, Windhoek, Namibia. Geological Survey of Namibia. CD-ROM.

Ramsay, C.R., Ridgway, J., 1977. Metamorphic patterns in Zambia and their bearing on problems of tectonic history. Precambrian Research 4, 321–337.

Raybould, J.G., 1978. Tectonic controls on Proterozoic stratiform mineralisation. Transactions of the Institution of Mining and Metallurgy 87, B79–B86.

Reeve, W.H., 1963. The geology and mineral resources of northern Rhodesia. Geological Survey of Northern Rhodesia Bulletin 1, 213.

Ripperdan, R.L., 2001. Stratigraphic variation in marine carbonate carbon isotope ratios. In: Valley, J.W., Cole, D.R. (Eds.), Stable Isotope GeochemistryReviews in Mineralogy and Geochemistry, vol. 43, pp. 637–662.

Robinson, B.W., Kusakabe, M., 1975. Quantitative preparation of sulfur dioxide, for $^{34}S/^{32}S$ analyses, from sulfides by combustion with cuprous oxide. Analytical Chemistry 47, 1179–1181.

Roedder, E., 1984. Fluid inclusions. Reviews in Mineralogy 12, 644.

Samama, J.C., Mapani, B.S.E., Tembo, D., in press. Report on the typical features of the Kabwe zinc lead deposit, Republic of Zambia. Their use in mineral exploration. — Geological Survey of Zambia and Geosum Company (France).

Sangster, D.F., 2003. A special issue devoted to nonsulfide zinc deposits: a new look. Economic Geology 98, 683–684.

Scholle, P.A., Halley, R.B., 1985. Burial diagenesis: out of sight, out of mind! SEPM Special Publication 36 "Carbonate Cements", pp. 309–334.

Schwarcz, H.P., Burnie, S.W., 1973. Influence of sedimentary environment on sulphur isotope ratios in clastic rocks: a review. Mineralium Deposita 8, 264–277.

Shepherd, J.P., Rankins, A.H., Alderton, D.H.M., 1985. A Practical Guide to Fluid Inclusion Studies. Blackie and Sons, Glasgow. 239 pp.

Skerl, A.C., 1934. Vanadium at the Rhodesia Broken Hill. Mineralogical Magazine 50, 280–283.

Sliwa, A., Podemski, M., in press. Kabwe West PL 142, final report. ZIMCO Limited, MINEX Department., 9 pp.

Speak, S.J., 1919. The lead–zinc deposits at the Rhodesia Broken Hill Mine, northern Rhodesia. The Mining Magazine 21, 203–209.

Spencer, L.J., 1908. On hopeite and other zinc phosphates and associated minerals from the Broken Hill mines, north-western Rhodesia. Mineralogical Magazine XV, 1–38.

Spencer, L.J., 1927. South African occurrences of willemite and some other zinc minerals in ultra-violet rays. Mineralogical Magazine 21, 388–396.

Sweeney, M.A., Binda, P.L., 1989. Mineralization controls and source of metals in the Lufilian fold belt, Shaba, (Zaire), Zambia, and Angola — a discussion. Economic Geology 84, 223–224.

Sweeney, M.A., Burnard, P., Vaughan, D.J., Kamona, F., 1990. A zonation in Central African metallogenesis: implications for base metal mineralisation in Central Zambia. In: Rocci, G., Deschamps, M., (Coordinators.), Recent data in African earth sciences. CIFEG Occasional Publication 1990/22, Nancy, p. 317–320.

Sweeney, M.A., Patrick, R.A.D., Vaughan, D.J., Turner, P., 1991. The nature and genesis of the willemite deposits of Zambia. In: Pagel, M., Leroy, J.L. (Eds.), Source, Transport and Deposition of Metals. Balkema, Rotterdam, pp. 139–142.

Takeno, S., 1975. The pseudobinary system briartite–chalcopyrite. Neues Jahrbuch für Mineralogie Monatshefte 294–299.

Taylor, J.H., 1954. The lead–zinc–vanadium deposits at Broken Hill, northern Rhodesia. Colonial Geology and Mineral Resources 4, 335–365.

Taylor, J.H., 1958. The formation of supergene galena at Broken Hill, northern Rhodesia. Mineralogical Magazine 31, 908–913.

Taylor Jr., H.P., 1979. Oxygen and hydrogen isotope relationships in hydrothermal mineral deposits, In: Barnes, H.L. (Ed.), Geochemistry of Hydrothermal Ore Deposits, 2nd ed. Wiley-Interscience, New York, pp. 236–277.

Thompson, T.M., Beaty, D.W., 1990. Geology and the origin of ore deposits in the Leadville District, Colorado: part II. Oxygen, hydrogen, carbon, sulphur, and lead isotope data and development of a genetic model. Economic Geology Monographs 7, 156–179.

Tuke, M.F., in press. The schistose dolomite and Mine Club fault. Zambia Broken Hill Mine.

Unrug, R., 1988. Mineralization controls and sources of metals in the Lufilian fold belt, Shaba (Zaire), Zambia, and Angola. Economic Geology 83, 1247–1258.

Unrug, R., 1996. The assembly of Gondwanaland. Scientific results of IGCP Project 288: Gondwanaland sutures and fold belts. Episodes 19, 11–20.

Whyte, W.J., 1966. Geology of the Broken Hill Mine, Zambia. Symposium on Lead–Zinc Deposits in Africa: Association of African Geological Surveys, Tunis Meeting, April 1966, vol. 23, pp. 395–425.

Wood, S.A., Samson, I.M., 2006. The aqueous geochemistry of gallium, germanium, indium and scandium. Ore Geology Reviews 28, 57–102.

Zartman, R.E., Doe, B.R., 1981. Plumbotectonics — the model. Tectonophysics 75, 135–162.

Zealley, A.E.V., 1912. A mineral survey of the zinc and lead deposits of Broken Hill, northern Rhodesia. South African Journal of Science 8, 389–398.